Imperial College London

MRes Individual Project

Imperial College London

Department of Surgery and Cancer

The Use of 3D Reconstruction and Virtual Reality to Support Prospective Bariatric Surgery Patients

Author:
Yuze Wang

Supervisor:
Prof. Fernando Bello
Nazrin Assaf

A thesis submitted in partial fulfilment of the requirements for the degree of MRes in Medical Robotics and Image Guided Intervention and for the Diploma of Imperial College London

September 15, 2023

Abstract

Background As the prevalence of obesity surges, an increasing number of individuals are resorting to bariatric surgery to safeguard their health. While 3-D reconstruction and virtual reality emerge as potent tools for bolstering psychological support to these patients, thereby enhancing their body image satisfaction and the overall effectiveness of interventions, challenges persist. The prolonged nature of the reconstruction process, intricate procedures, limited accuracy in the reconstructions, and a lack of variability in the presentation of the reconstructed results have impeded the widespread adoption of this promising approach.

Purpose This research endeavors to enhance the precision of 3-D reconstructions, streamline the duration of the reconstruction process, simplify the intricacies involved in the reconstruction procedure, and diversify the modes of presenting reconstructed outcomes.

Methods An armature iterative algorithm was introduced to precisely modulate the dimensions of distinct body regions to attain a targeted percentage of total weight reduction. Concurrently, a skin fold simulation algorithm was developed, harnessing the principles of a mass-spring model to emulate post-weight loss skin sagging. The study also engaged in a quantitative assessment of the 3D scanning technique's accuracy and instituted various VR perspectives.

Results Visualization was achieved for varying percentages of weight loss paired with distinct levels of skin folds. Enhanced 3D scanning techniques were identified through a quantitative analysis. A hybrid approach combining both first-person and third-person viewpoints was employed to optimize the VR experience for participants.

Conclusion By integrating the two algorithms within the 3D reconstruction phase, the overall procedure time was significantly reduced to 15% of conventional methods. This streamlined approach not only simplifies the process for researchers but also enhances the accuracy of reconstruction outcomes. Consequently, a more comprehensive representation of post-weight loss morphological changes is now attainable.

Word Count (without appendices) : 11449

Word Count (with appendices) : 11991

Acknowledgements

First and foremost, I owe a profound debt of gratitude to Prof. Fernando Bello, my mentor and guiding force throughout this research journey. His unwavering faith in me and invaluable insights during challenging times were the bedrock upon which this project was built. Without his guidance, this topic would not have come to fruition.

A special mention must be made of Ms Nazrin Assaf and her friend. Nazrin's clinical expertise provided me with the necessary direction, ensuring I remained on the right path. Her own experiences in this field have been a source of inspiration. I extend my sincere thanks to Nazrin's friend, who generously contributed vital raw data, aiding in the validation of my algorithm.

Dr Reza Haghighi Osgouei's technical mentorship was indispensable. His consistent support, both in terms of technical direction and uplifting words, instilled in me the confidence to persevere. I am also deeply appreciative of Mr Agni Lahiri, whose technical advice was instrumental to my research.

I extend my heartfelt thanks to Prof. Daniel S Elson, Dr. George Mylonas, and Dr. Stamatia Giannarou. Their tutelage during various courses and group research projects equipped me with the knowledge and experience required to undertake the challenges of this individual project.

My colleagues, Miss Runmeng Ding and Mr Shun Yao deserve special recognition. Our camaraderie in the research group, even while working on distinct topics, was a source of motivation and mutual encouragement.

I'm profoundly thankful to Ms Hui Tian and Mr Qiang Wang for their unwavering support, which granted me the liberty to immerse myself completely in my research.

Lastly, my sincere gratitude goes to Imperial College for granting me this invaluable opportunity. This project serves as a foundation upon which I aim to build further research.

List of Abbreviations

WHO	World Health Organization
BMI	Body Mass Index
NHANES	National Health and Nutrition Examination Survey
NIH	National Institutes of Health
ASMBS	American Society for Metabolic and Bariatric Surgery
SG	Sleeve Gastrectomy
RYGB	Roux-en-Y Gastric Bypass
AGB	Adjustable Gastric Banding
BPD-DS	Biliopancreatic Diversion with Duodenal Switch
VR	Virtual Reality
IVR	Immersive Virtual Reality
VCSEL	Vertical Cavity Surface Emitting Lasers
SPAD	Single-Photon Avalanche Diodes
TWL	Total body Weight Loss
MSM	Mass-Spring Model
MAE	Mean Absolute Error

Contents

1 Introduction and Literature Review **6**

1.1 Clinical Background 6

1.1.1 Obesity 6

1.1.2 Bariatric Surgery 7

1.1.3 Body Image 13

1.2 The overview of existing evidence 15

1.2.1 Psychological Support in Bariatric Surgery 15

1.2.2 Virtual Reality(VR) in Healthcare 16

1.2.3 Anthropometry and 3D Scanning Technology 17

1.2.4 Post-operative body changes 18

1.2.5 Relevant Existing Research 19

1.3 Aims and Objectives 19

1.3.1 Aims 19

1.3.2 Objectives 20

2 Methods **21**

2.1 3D Scanning 21

2.1.1 3D Scanning Application 21

2.1.2 3D Scanning Environment 23

2.1.3 3D Scanning Method 23

2.2 3D Reconstruction 24

2.2.1 Armature Design and Binding 24

2.2.2 Armature Resizing Algorithm 26

2.2.3 Skin Fold Areas 28
2.2.4 Skin Folds Simulation Algorithm 29
2.3 VR Application 31
2.3.1 VR Scenes 31
2.3.2 VR Configuration 34

3 Results **36**
3.1 3D Scanning 36
3.2 3D Reconstruction 38
3.2.1 Body Size Reduction 38
3.2.2 Skin Fold Simulation 39
3.2.3 Whole Body Simulation 46
3.3 VR Applications 49

4 Discussion **52**
4.1 Conclusion and Achievements 52
4.2 Limitation 53
4.3 Future Work 54

A Armature Resizing Code **62**

B Skin Fold Simulation Code **66**

List of Figures

1.1 Sleeve Gastrectomy 9
1.2 Roux-en-Y Gastric Bypass 10
1.3 Adjustable Gastric Band 11
1.4 Biliopancreatic Diversion with Duodenal Switch 12
1.5 Single Anastomosis Duodeno-Ileal Bypass with Sleeve Gastrectomy 13

2.1 ”Polycam” scanning test results 21
2.2 ”3D Scanner APP” scanning test results 22
2.3 ”Scaniverse” scanning test results 22
2.4 Body Armature 25
2.5 ”Head” armature-controlled parts (the degree of redness indicates the degree of influence of the corresponding armature) 25
2.6 Skin Fold Areas(eg: Left Upper Arm) 29
2.7 Swimming Pool Scene 32
2.8 Beach Scene 33
2.9 Cloakroom Scene 33
2.10 Oculus Quest 2 VR Headset and Hand Controllers 34

3.1 Actual Measurements 38
3.2 Facial Eigenvalue 38
3.3 3D Scanning Model Measurements(eg: 1-min flat) 38
3.4 Trends in body size reduction (Front View) 39
3.5 Trends in body size reduction (Side View) 39
3.6 Skin fold grading of the arm (Example) 41

3.7 Arm skin fold simulation grading 42
3.8 Skin fold grading of the thigh (Example) 43
3.9 Thigh skin fold simulation grading 43
3.10 Skin fold grading of the abdomen (Example) 44
3.11 Abdomen skin fold simulation grading 44
3.12 Skin fold grading of the Mammary Gland (Example) 45
3.13 Mammary gland skin fold simulation grading (Front View) 45
3.14 Mammary gland skin fold simulation grading (Side View) 45
3.15 Whole Body Simulation 46
3.16 Original model and post-bariatric surgery simulation model for Participant 1 47
3.17 Original model and post-bariatric surgery simulation model for Participant 2 47
3.18 Original model and post-bariatric surgery simulation model for Participant 3 48
3.19 Original model and post-bariatric surgery simulation model for Participant 4 48
3.20 Original model and post-bariatric surgery simulation model for Participant 5 48
3.21 Original model and post-bariatric surgery simulation model for Participant 6 49
3.22 Swimming Pool Scenario Third View 49
3.23 Swimming Pool Scenario First View 50
3.24 Cloakroom Scenario Third View 50
3.25 Cloakroom Scenario First View 50
3.26 Beach Scenario Third View 51
3.27 Beach Scenario First View 51

List of Tables

3.1 Comparison of Eigenvalue Positions between Actual and Scanned Measurements 37

3.2 Scale Factors and Percentage Reductions for Each Model 40

Chapter 1

Introduction and Literature Review

1.1 Clinical Background

1.1.1 Obesity

In recent decades, global health agencies and researchers have shown growing concern over the worldwide rise in obesity levels. As early as two decades ago, the World Health Organization (WHO) identified the mounting obesity rates as a 'global epidemic'[1]. However, notwithstanding this acknowledgment, the prevalence of individuals considered overweight (defined by a body mass index (BMI) equal to or exceeding $25 kg/m^2$) and those classified as obese (with a BMI equal to or surpassing $30 kg/m^2$) has relentlessly risen[2, 3]. Data from 2016 underscores this concerning trajectory, revealing that approximately 1.9 billion adults, or 39% of the world's adult demographic, were overweight. Alarmingly, over 650 million of these individuals, representing 13% of this population, met the criteria for obesity, with some nations reporting rates that eclipsed 50%[3]. This escalating trend is not limited to adults; it further extends to younger populations. In the same year, an estimated 41 million children under the age of five, as well as 340 million children and adolescents between the ages of 5 and 19, were categorized as overweight or obese[4]. It's noteworthy to highlight that while developed countries have seen a slight deceleration in obesity growth rates, developing nations are witnessing a rapid rise, leading to the sobering realization that no nation has genuinely reversed this epidemic. Projections, based on current data, suggest a potential increase in obesity prevalence by an additional 33% come 2030[5].

A deeper exploration into BMI distribution over the years yields a compelling narrative. Although there has been a general shift towards higher BMIs across the board, it's the upper echelons of this spectrum that have witnessed the most

pronounced changes. A seminal study, encompassing data collected as part of the National Health and Nutrition Examination Survey (NHANES) from American adults aged between 20 to 74 years during 1976–1980 and 1999–2004, reveals a marked rightward skew in BMI distribution[6]. This shift was concomitant with a twofold rise in adult obesity rates (from 15.0% during 1976–1980 to 32.9% by 2003–2004). Moreover, those classified as morbidly obese (with BMIs of $40 kg/m^2$ or higher) saw their proportions amplify threefold, from a mere 1.4% during 1976–1980 to 5.1% by 2003–2004[6]. This trajectory mirrors observations from other affluent nations such as the UK[7], and other high-income regions[8, 9]. Forecasts based on these trends predict an alarming escalation in morbid obesity, with anticipations of a 130% increase between 2010 to 2030[5]. Interestingly, this phenomenon isn't geographically confined. For instance, China and India reported the largest obese child populations globally in 2015, and together with the US, China topped the charts for obese adults[10]. Notably, regions such as Africa and Asia have recorded the most accelerated growth in obesity rates[11].

To effectively address this epidemic, it is vital to comprehend its root causes. Simplistically, obesity emerges from a prolonged positive energy balance, where caloric intake surpasses expenditure. Primary factors influencing this balance are dietary habits, specifically the energy density and volume of consumed food, juxtaposed against physical activity levels in terms of type, intensity, and regularity. An imbalance, favoring energy intake over expenditure, invariably leads to weight accumulation.

The ubiquity and magnitude of obesity underscore its positioning as a paramount health concern, transcending national boundaries and development indices. Recognized as a chronic, progressive disease, obesity brings with it an array of health complications, with elevated morbidity and mortality rates[12, 13, 14]. Beyond these physiological impacts, obesity can significantly impede an individual's quality of life, predisposing them to a gamut of chronic conditions that include, but are not limited to, cardiovascular diseases, type 2 diabetes, and various cancers[15, 16, 17]. Given this background, the subsequent sections will delve into targeted interventions and strategies to curtail this burgeoning global health crisis.

1.1.2 Bariatric Surgery

Over the past few decades, the medical community has recognized bariatric surgery as a pivotal therapeutic intervention for treating severe obesity and its myriad associated comorbidities. Commonly referred to as weight loss surgery or metabolic surgery, bariatric surgical procedures aim to effectuate substantive

weight reduction and consequently mitigate weight-induced medical complications. In 1991, a consensus panel convened by the National Institutes of Health (NIH) delineated the eligibility criteria for candidates of this surgical intervention[18]. As per their guidelines, bariatric surgery is deemed appropriate for individuals exhibiting a BMI exceeding 40. Furthermore, it is also recommended for those with a BMI range of 35-40, contingent on the presence of accompanying comorbid conditions.

Recent statistical reports from the American Society for Metabolic and Bariatric Surgery (ASMBS) reveal that the US witnessed an approximate 228,000 bariatric surgeries in 2017 alone[19]. A deeper probe into the types of surgeries performed showcases that the vertical sleeve gastrectomy (SG) dominated the list, accounting for over 59% of the procedures. The Roux-en-Y gastric bypass (RYGB) comprised close to 18%, while revisional procedures formed a bit over 14%. The residual percentage was distributed among other surgical techniques, including adjustable gastric banding (AGB), biliopancreatic diversion with duodenal switch (BPD-DS), and a medley of niche procedures, which encompass endoscopic, aspirational, and vagal-stimulating methodologies.

One of the defining trajectories in the bariatric surgical landscape has been the marked enhancement in its safety profile in the last two decades. This favorable transition can be attributed, in significant part, to the extensive adoption of laparoscopy[20] and the integration of other minimally invasive surgical techniques. As a consequence of these advancements, the mortality rates associated with these surgeries have plummeted, and many complications that were erstwhile deemed routine have been relegated to rarity[21]. In its current state, bariatric surgery stands on a safety pedestal, rivaling, if not surpassing, the safety metrics of gallbladder surgeries and other standard surgical procedures[22].

Given the burgeoning global obesity crisis, understanding the relevance and efficacy of bariatric surgery is paramount. The aforementioned data underscores the procedure's significance, not just as a weight reduction mechanism, but as a comprehensive therapeutic approach to address the multifaceted health challenges precipitated by obesity.

Sleeve Gastrectomy(SG)

The Laparoscopic Sleeve Gastrectomy(Fig.1.1), often termed the "sleeve", involves removing about 80% of the stomach. The stomach left behind is banana-shaped and smaller in size.

The diminished stomach restricts the amount of food and liquid consumed, thereby reducing calorie intake. As the part of the stomach responsible for the production of the majority of the "hunger hormone" is removed, this surgery impacts metabolism by reducing hunger, increasing the sensation of fullness, and assisting the body to achieve and sustain a healthy weight and control blood sugar levels. Due to its straightforward nature, the operation is considered very safe, avoiding potential complications related to procedures on the small intestine.

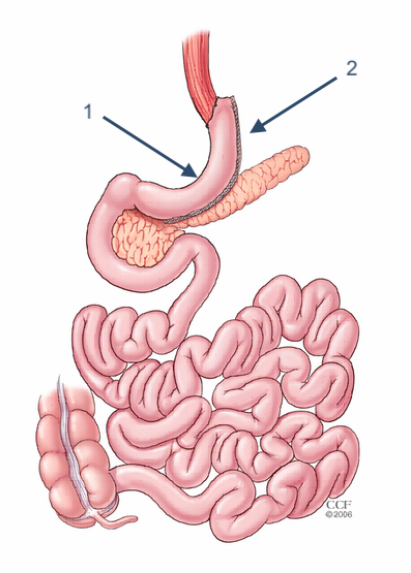

Figure 1.1: Sleeve Gastrectomy

Roux-en-Y Gastric Bypass (RYGB)

The Roux-en-Y Gastric Bypass(Fig.1.2), commonly known as the "gastric bypass", has been conducted for over 50 years, and its laparoscopic technique has been improved since 1993. It's a frequently performed operation and effectively addresses obesity and related diseases. The term originates from French and translates to "in the shape of a Y".

The gastric bypass functions in multiple ways. Similar to other bariatric procedures, the newly formed stomach pouch is smaller, thus limiting food intake and calorie consumption. Moreover, the initial segment of the small intestine doesn't come in contact with food, leading to less absorption. Crucially, the redirection of food passage through the gastrointestinal tract significantly reduces hunger, enhances the sensation of fullness, and assists the body in reaching and maintaining a healthy weight. Hormonal and metabolic health benefits often lead to the amelioration of adult onset diabetes even before weight loss is noticed. The procedure also aids patients suffering from reflux (heartburn), often leading to quick symp-

tom relief. Alongside making suitable food choices, patients are advised to refrain from tobacco products and non-steroidal anti-inflammatory drugs (NSAIDs) like ibuprofen and naproxen.

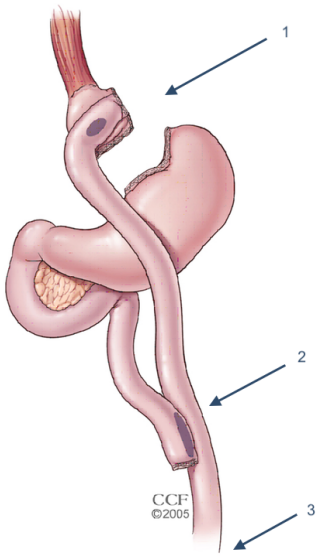

Figure 1.2: Roux-en-Y Gastric Bypass

Adjustable Gastric Band (AGB)

The Adjustable Gastric Band(Fig.1.3) is a silicone device positioned around the top section of the stomach to restrict food intake. It's been available in the United States since 2001. Its impact on obesity-related diseases and long-term weight loss is less significant compared to other procedures, thus its usage has decreased over the past decade.

The feeling of satiety is contingent upon the size of the opening between the pouch and the rest of the stomach, which can be adjusted via fluid injections into a port under the skin. Food passes through the stomach normally but is restrained by the band's smaller opening. Its effectiveness against type 2 diabetes is less pronounced and it has modest effects on metabolism.

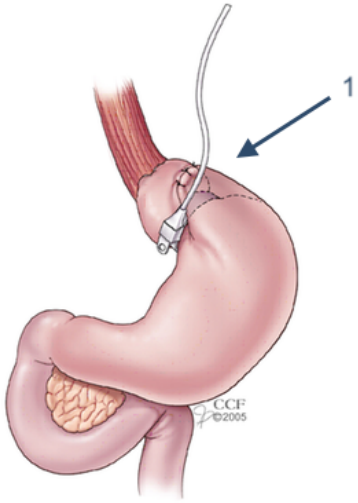

Figure 1.3: Adjustable Gastric Band

Biliopancreatic Diversion with Duodenal Switch (BPD/DS)

The Biliopancreatic Diversion with Duodenal Switch(Fig.1.4), or BPD-DS, starts with the formation of a tube-shaped stomach pouch akin to the sleeve gastrectomy. It resembles the gastric bypass, but a larger portion of the small intestine is bypassed.

The downsized, banana-shaped stomach allows less food consumption. The food stream bypasses approximately 75% of the small intestine, the highest amount in any routinely performed approved procedures, leading to a considerable reduction in calorie and nutrient absorption. Post-surgery, patients must consume vitamins and mineral supplements. Even more so than the gastric bypass and sleeve gastrectomy, the BPD-DS influences intestinal hormones in a way that lessens hunger, increases fullness, and aids in blood sugar control. It's deemed the most effective approved metabolic procedure for treating type 2 diabetes.

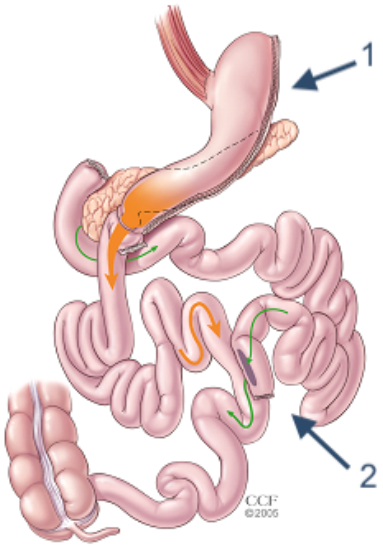

Figure 1.4: Biliopancreatic Diversion with Duodenal Switch

Single Anastomosis Duodeno-Ileal Bypass with Sleeve Gastrectomy (SADI-S)

The Single Anastomosis Duodenal-Ileal Bypass with Sleeve Gastrectomy(Fig.1.5), referred to as SADI-S, is the latest procedure to receive endorsement from the American Society for Metabolic and Bariatric Surgery. While it bears similarities to the BPD-DS, the SADI-S is simpler and quicker to perform as there's only one surgical bowel connection.

When the patient consumes food, it passes through the pouch and directly into the latter part of the small intestine. The food then blends with digestive juices from the upper section of the small intestine. This process ensures enough absorption of vitamins and minerals to maintain nutritional health. This surgery provides effective weight loss along with reduced hunger, increased satiety, controlled blood sugar levels, and improvement in diabetes.

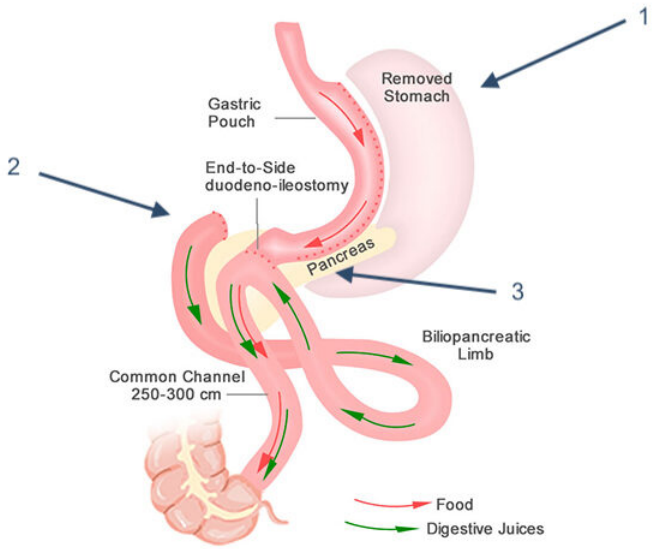

Figure 1.5: Single Anastomosis Duodeno-Ileal Bypass with Sleeve Gastrectomy

1.1.3 Body Image

Body Image Before Bariatric Surgery

In the realm of obesity research, there exists a burgeoning body of evidence delineating the psychosocial hardships endured by individuals grappling with obesity, especially those contemplating bariatric surgery as a potential intervention. One of the most striking domains impacted by these adversities is body image[23]. Current societal constructs present a paradigm that is overwhelmingly skewed towards thinness. This bias, augmented by the media's consistent portrayal of svelte figures as the zenith of happiness and success, cultivates an environment of weight-related prejudice. Such a setting can exacerbate feelings of inadequacy and self-deprecation in individuals with obesity[24]. Profoundly, several among these individuals resonate with sentiments of being metaphorically "ensnared" within their expansive physiques, an evocative manifestation of their emotional turmoil[25].

The magnitude of societal bias targeting individuals opting for bariatric surgery is palpable. Anecdotal evidence from obese patients paints a disheartening tableau of persistent discrimination rooted in weight-based prejudice[26]. Recurrent narratives echo experiences marred by apprehension or mortification during public dining, judgments anchored in their grocery choices, and subpar interactions with customer service personnel[27]. Such external stigma doesn't merely remain an external experience; it often permeates their self-worth, leading to a negative internalized self-perception[28]. Qualitative analyses further illuminate the pro-

found dissatisfaction these individuals experience upon confronting their reflections or photographic likenesses[29]. In a telling statistic, approximately 32% of bariatric surgery aspirants highlight the amelioration of their self-image as a primary impetus behind their surgical decision[30].

Supplementing these insights is the revelation that many individuals on the precipice of bariatric surgery bear extensive histories riddled with persistent dieting endeavors and resultant weight vacillations, further destabilizing their body image[31]. A particular study involving bariatric surgery candidates unearthed instances where participants endured up to fifteen unfruitful dieting attempts, punctuated by recurring weight oscillations[32]. Furthermore, the cyclical nature of dieting, characterized by intermittent weight loss and regain, might inadvertently catalyze a cumulative weight augmentation over prolonged durations[33].

Building on this foundation, it becomes paramount to posit that cultivating a positive body image pre-operatively can act as a linchpin in the surgical journey of bariatric patients. Establishing an affirmative self-perception could potentially serve as a robust psychological scaffold, bolstering patients' resilience and fortifying their commitment to successful weight loss post-surgery. It's imperative to underscore the role of holistic pre-operative counseling that accentuates body positivity, thereby fostering an environment conducive to both physical and mental well-being during the bariatric journey.

Body Image After Bariatric Surgery

Following bariatric surgery, extant research underscores a mosaic of perceptions and emotions that patients navigate as they grapple with their transforming physique, metaphorically described as the weight "dissolving"[28]. A salient segment of these patients delineates an elevation in self-worth and a more favorable body image, complemented by diminished feelings of mortification post-operatively[34]. Such narratives often echo with sentiments of astonishment, exhilaration, and jubilation upon witnessing the continual diminution of their bodily form[35]. Nevertheless, this transformative journey is not devoid of complexities[36]. The post-operative phase is punctuated with exacting self-care regimens that require unwavering adherence. These stipulate a plethora of dietary protocols, encapsulating protein consumption, portion moderation, recurrent meal schedules, supplemental intake, and routine clinical consultations. In the face of such rigorous weight decline, a subset of patients confront challenges in maintaining this reduced weight threshold. They grapple with potential weight rebound and are often besieged by residual sagging skin - a physical aftermath frequently deemed

aesthetically displeasing[37, 38].

Furthermore, a dissection of the literature elucidates two critical impediments intertwined with body image that could potentially thwart the fruition of post-operative weight loss objectives[28]. The inaugural challenge emanates from the potential ebbing of social backing subsequent to the surgical intervention. An illustrative testament to this dynamic is encapsulated in sentiments such as, "He castigates me for selecting the facile solution," alluding to the surgical route[28]. Altered dynamics in marital or intimate affiliations post-bariatric surgery have been empirically tethered to transformations in body image and weight trajectories[39]. The stark metamorphosis marked by substantial weight reduction, juxtaposed with sagging epidermal layers, abdominal droop, and pendulous breasts, might culminate in a dissonant perception of their metamorphosed selves[28].

Additionally, the scholarly realm has spotlighted a nuanced clinical phenomenon termed "mind-body lag." Herein, despite tangible weight diminution, the cognitive representation retains an obese body image, engendering a discord between the physical and psychological self[40].

In light of these multifaceted post-operative challenges, the imperative of fostering a positive body image during the pre-operative phase gains paramount significance. Establishing a robust, affirmative self-perception pre-surgically can act as an instrumental bulwark, aiding patients to adeptly navigate the multifarious physiological and psychological terrains post-surgery. Comprehensive pre-operative counseling accentuating body positivity and realistic expectations could substantially ameliorate the transition, bolstering patients' equanimity as they tread the transformative journey of post-operative weight loss.

1.2 The overview of existing evidence

1.2.1 Psychological Support in Bariatric Surgery

Psychological support plays a vital role in the journey of bariatric surgery patients. Beginning from the decision to have surgery through to recovery and lifestyle adaptation, patients can benefit significantly from professional psychological services.

Prior to surgery, psychological evaluations are commonly conducted to assess the patient's readiness for the lifestyle changes required by the procedure[41]. These assessments aim to identify any potential mental health issues that could hinder post-operative recovery and weight loss success. It's important to address

any concerns related to eating disorders, substance abuse, or untreated psychiatric conditions like depression or anxiety.

Psychological support is also beneficial post-surgery. The physical changes that accompany significant weight loss often prompt a series of emotional and psychological changes. Patients may struggle with body image issues, emotional eating patterns, or adjusting to societal reactions to their new physique. Counseling and support groups can provide patients with coping strategies, while fostering a sense of community and shared experience. These support avenues also offer a platform for patients to share their concerns and fears, which can be especially reassuring for those who feel isolated or overwhelmed[42].

Additionally, long-term psychological support is crucial to help patients maintain the necessary lifestyle changes, including dietary habits and regular physical activity[43]. Reinforcing these habits is essential to prevent weight regain, a common concern for many post-surgical patients. Cognitive behavioral therapy, mindfulness techniques, and motivational interviewing are some of the tools psychologists may use to help patients stay on track.

1.2.2 Virtual Reality(VR) in Healthcare

The development and application of VR provide solutions to improve patient prognosis. This technology has been widely recognized in medical services. This is through anxiety control, pain management, patient education, physical recovery and behavioral cognitive therapy, body image expectations and avoidance of bad habits in surgeries[44, 45]. VR is a computer simulation system that allows the creation and experience of virtual worlds. According to its ability to participate, users can be immersive or non-immersive [46]. Immersive virtual reality(IVR) in medical simulation comes into focus because it is created by surrounding the user of the VR system with images, sound or other stimuli that provide an engrossing total environment. IVR is often applied in different ways. Headset display and simple headphones are the common devices used in IVR applications today[45].

VR for Bariatric Surgery Patients

VR presents a novel avenue for bolstering behavioural and emotional sustenance to patients on this transformative journey. Distinctly, VR has the potential to be a pivotal anchor in realising and preserving weight loss outcomes in the long-term. Recent scholarly investigations into virtual reality psychotherapy[47] and body image intervention[48] elucidate their efficacy in augmenting weight

management strategies and fortifying compliance to structured weight loss regimens.

However, a lacuna in current research is the paucity of studies exploring the application of these VR methodologies specifically to the post-operative bariatric cohort. Given this contextual backdrop, an intriguing question arises: How might post-surgical bariatric patients benefit from these VR-infused interventions? Especially with the proliferation of economically accessible and intuitively designed VR headset apparatuses, there emerges the feasibility of domiciliary implementation of such therapies.

Incorporating these state-of-the-art VR mechanisms into the post-operative care regimen of bariatric patients could engender a multi-dimensional therapeutic milieu. Such an environment would address the physiological aspects of weight management and cater to the nuanced psychological intricacies that invariably accompany the post-surgical phase.

1.2.3 Anthropometry and 3D Scanning Technology

Anthropometry, an application of metrology that is inherently focused on the measurement of the human physique, encompasses a holistic methodology that incorporates data collection, recording, analysis, and summarization. This practice, at its core, aims to quantify the human morphology through precise physical measurements of various body segments[49].

Methods for procuring anthropometric data manifest in various forms. While traditional modalities, utilizing tools such as calipers and tape measures, dominate manual measurements, technological advancements have ushered in 3D scanning as a viable alternative for automated measurements. However, the crux of obtaining reliable measurements, irrespective of the methodology employed, lies in the adherence to established standards, which meticulously define the requisite postures and demarcate body landmarks for precision[50]. Although manual measurements have been hailed as the gold standard due to their longstanding application, emerging literature emphasises that human experts are essentially at the same level of accuracy as that demonstrated by 3D scanners. In juxtaposition, 3D scanners often surpass in terms of repeatability, augmented by their innate rapidity wherein scans are executed within mere seconds[51].

Building on the aforementioned paradigms of anthropometry, my approach to recreating a patient's post-operative likeness was deeply informed and influenced by these principles. It was imperative to rely on empirical data that could offer a

robust and objective representation of the patient's pre-operative physical stature. To this end, I elected to employ 3D scanning as the primary instrument for data acquisition, leveraging its prowess in accuracy and speed, thereby ensuring that the resultant reconstruction was both faithful to the original and grounded in empirical rigor.

LiDAR

Lidar, short for "light detection and ranging" or "laser imaging, detection, and ranging", is a technique used to gauge distances by illuminating a target with a laser and then calculating the time taken for the reflected light to travel back to its source[52]. The latest Apple smartphones and tablets have integrated this technology, facilitating 3D modeling. Presently, Apple employs 9XX nm VCSELs (Vertical Cavity Surface Emitting Lasers) and SPADs (Single-Photon Avalanche Diodes). VCSELs are gaining traction in 3D scanning applications due to their capacity to generate sub-nanosecond pulses. These lasers work in tandem with SPADs, specialized detectors that can accurately measure distances regardless of the reflectivity of the object[53, 54]. The precision of the resulting 3D model hinges on both internal and external variables. While device hardware and software are the internal aspects, external elements include lighting conditions, the texture of the surface, and the scanning approach employed. Notably, direct sunlight can interfere with LiDAR measurements, as the intense sunlight can overwhelm the LiDAR's detector, contrasting sharply with the fainter return signal from the LiDAR[55].

1.2.4 Post-operative body changes

In an endeavour to critically assess the ramifications of bariatric surgery, a discernible variability in weight loss outcomes emerges among the patient cohort. Several pivotal factors play a determinative role in influencing postoperative weight loss outcomes. These encompass the type of surgical intervention employed, the gender demographics of the patient, and their financial capacities[56]. A meticulous scrutiny of the accumulated data reveals a stratified picture: patients who underwent RYGB manifested an average total body weight loss (TWL) of 31.2% within the inaugural postoperative year. This statistic stands in juxtaposition to the 25.2% TWL observed among the SG recipients and the comparatively lower 13.7% registered for those who underwent AGB during the equivalent temporal window[57].

An intriguing empirical endeavour leveraged the prowess of a 3D photon scan-

ner, propounding a non-invasive paradigm to chronicle both holistic and regional morphological shifts in patients, accompanied by nuanced fluctuations in parameters such as circumference and length, subsequent to their surgeries[58]. The elucidations derived from this seminal study offer profound insights, imbuing the current research discourse with pivotal cues, particularly when navigating the challenges of simulating the postoperative anatomical transformations of patients.

Furthermore, a consequential corollary often affiliated with bariatric surgical interventions is the evolution of skin folds, manifested to varied extents across patients[59]. The genesis of these dermatological contours can be traced back to an amalgamation of antecedents, notably the patient's antecedent BMI, age, and gender. Such folds predominantly emerge across anatomical regions like the abdomen, arms, and thighs. In female patients, a pronounced manifestation is observed in the mammary region[60]. This phenomenon further underscores the intricacies involved in the accurate simulation of postoperative body transformations.

1.2.5 Relevant Existing Research

A pilot clinical study was conducted by Assaf to ascertain if 3D reconstruction and VR could serve as effective tools for psychological support to these patients[61]. Seven participants from the specialist weight management bariatric pathway underwent 3D scanning, which produced images reflecting 15% and 25% weight loss. These images were then presented via VR, followed by peer group workshops. The results were promising; participants indicated improved understanding of post-surgery body changes, suggesting that this method provides a realistic rather than an idealistic expectation. The consensus was that this approach would assist patients in adapting to their altered body image post-surgery. This pioneering study highlights the potential of 3D reconstruction and VR in setting realistic body change expectations post-bariatric surgery, aiming to bolster both psychological and clinical results.

1.3 Aims and Objectives

1.3.1 Aims

The aim of this project is to simulate what an obese patient would look like after weight loss surgery using 3D real-life portrait scanning, 3D model recon-

struction and virtual environment immersive experience. This is important for patients to develop a positive body image and increase their confidence in weight loss.

1.3.2 Objectives

1. To perform a complete and clear 3D scanning of the participant.

2. To determine the proportion of localised weight loss in each part of the body for a given proportion of the whole body's weight loss.

3. To determine the appearance of skin folds after weight loss.

4. To use appropriate software as well as models to reconstruct the patient's post-weight loss appearance at a certain scale.

5. To import the reconstructed model into diverse virtual environments.

Chapter 2

Methods

2.1 3D Scanning

3D scanning is the first step in the whole simulation process. In this session, we need to determine the scanning application, environment, and method.

2.1.1 3D Scanning Application

Based on our reviews, we selected three 3D scanning apps compatible with the iPad Pro (3rd Generation) (Apple Inc, California, USA). They are ”Polycam”, ”3D Scanner App” and ”Scaniverse”. We took the same scanning method and environment for each app for testing. This step is only to compare which of the different scanning applications works better, not to obtain scanning results.

(a) Front View (b) Side View

Figure 2.1: ”Polycam” scanning test results

(a) Front View (b) Side View

Figure 2.2: ”3D Scanner APP” scanning test results

(a) Front View (b) Side View

Figure 2.3: ”Scaniverse” scanning test results

From the above test results, we can visualise the following results. ”Polycam”(Fig.2.1) is generally good in appearance, but still has a lot of flaws in the details. There are artefacts at the top of the hair, the mesh of the hands is broken as well as the texture fit is very poor. Compared to the ”Polycam”, the ”3D Scanner APP” results(Fig.2.2) are much worse. Many holes and flaws can be seen in the shape profile. We think ”Scaniverse” has the best results(Fig.2.3). Both appearance, torso details and textures are excellent. Even the hands have slight artefacts, but this does not affect the subsequent reconstruction tasks. In addition, ”Scaniverse” can also export mesh to a variety of formats, including FBX, OBJ and PLY. In short, ”Scaniverse” beats the other two applications in terms of image quality, minimisation of motion artefacts and mesh file output format. Therefore, we will use ”Scaniverse” and design different scanning methods to improve the scanning results.

2.1.2 3D Scanning Environment

We selected the SiMMS laboratory at Chelsea and Westminster Hospital as the scanning site. As LiDAR scanning can be affected by sunlight contamination, especially backscattering noise. this is due to the background noise sunlight can be picked up by the LiDAR receiver thus interfering with the formation of the point cloud. In order to minimise this negative effect, we closed the blinds and only maintained the inherent uniform illumination of the room. However, to prevent any shadows from appearing on the 3D model, we used a ring light.

2.1.3 3D Scanning Method

We will use a circular trajectory with a 1.5m radius from the centre of the scan as the scanner's path of travel. The researcher performing the 3D scan had the ring light strapped to their head. The Apple iPad Pro was positioned so that the subject was always at the centre of the screen. Subjects were asked to stand on an "X" marking the centre of the scanning area, with their feet hip-width apart and their arms held flat.

We varied the length of the scan and the trajectory of the scanning device held by the researcher. The fidelity of the 3D avatar was compared to find the best scanning method.

Firstly, we designed the scanning duration as 1 minute, i.e. the researcher holding the scanning device took 1 minute to walk the circular route. The trajectory of the scanning device was flat scanning, i.e., the scanning device was always parallel to the person being scanned. We found that the overall results were good, but there would be some small defects of distortion in the face and obvious artefacts in the hair.

We then tried to increase the scanning time. That is, the scan duration was set to 2.5 minutes. The movement trajectory of the scanning device remained the same, and it was still a flat scan. We observe that the facial fidelity is significantly improved compared to the previous one, but the hair artefacts are still present.

Considering that the flat scanning mode of scanning neglects to capture the colour features of the top of the head. This time, we set the scanning device to move up and down, i.e., at the beginning of the scan and every quarter of the circular trajectory, the researcher slowly raised the scanning device to 45° diagonally above the subject, and then lowered it to the same position as before raising it to continue scanning. This time, we kept the scanning time constant by

still setting the scan length to 2.5 minutes. We found a significant reduction in hair artefacts.

Although we have found that boosting the scan time improves the accuracy of the scan. However, it is difficult for the participants to remain stationary for a longer period of time. The slightest movement of the subject will reduce the scanning accuracy. Therefore, we determined that the scanning time used in this study was 2.5 minutes, and the scanning device trajectory was to move up and down every quarter of a circular arc.

2.2 3D Reconstruction

In the 3D scanning section, we scanned the participants using the Scaniverse app on an Apple iPad Pro. The scanned mesh is then imported into Blender 3.4 in FBX format. In the 3D reconstruction section, we will reconstruct the mesh using Blender. Blender, as a 3D modelling software, offers a comprehensive suite of tools for reconstructing human body scans with high fidelity. Its robust physics engine ensures realistic simulations and interactions for complex human deformable meshes. Furthermore, its Python-driven architecture provides flexibility for custom scripts and automation, streamlining the reconstruction process and enabling advanced functionalities.

A new method of simulating the body shape and skin appearance of patients after weight loss will be proposed in this session.

2.2.1 Armature Design and Binding

Drawing from a comprehensive analysis of previous anthropometric body segmentation studies, a distinct armature tailored specifically for the objectives of the current investigation was conceived. The assemblage of body armatures was meticulously segmented into three primary regions, further subdivided into 18 detailed sections.

Specifically, the central trunk region encompassed sections such as the ”Head”, ”Neck”, ”Chest”, ”Abdomen”, ”Pelvis”, and ”Buttock”. The upper limb region was demarcated into the ”Left Upper Arm”, ”Right Upper Arm”, ”Left Forearm”, ”Right Forearm”, ”Left Hand”, and ”Right Hand”. Lastly, the lower limb region comprised the ”Left Thigh”, ”Left Calf”, ”Left Foot”, ”Right Thigh”, ”Right Calf”, and ”Right Foot”(Fig.2.4).

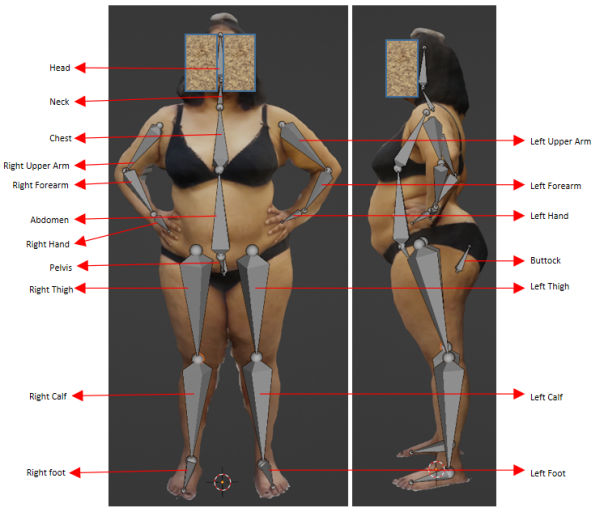

Figure 2.4: Body Armature

In the Blender software environment, these delineated armatures are bound to the mesh. Consequently, each armature segment directly manipulates its associated mesh portion(Fig.2.5). This intricate design and linkage facilitate granular and precise modulations of the human form, all orchestrated through this armature framework.

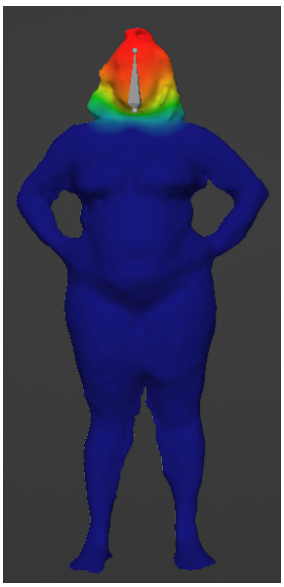

Figure 2.5: ”Head” armature-controlled parts (the degree of redness indicates the degree of influence of the corresponding armature)

2.2.2 Armature Resizing Algorithm

Developed in Python, this algorithm functions iteratively. It is geared to control the dimensions of the custom armature, simulating potential alterations in body shape after weight loss.

Volumetric Assessment of 3D Meshes

The core of the algorithm is to use the API in Blender to calculate the volume of the 3D human mesh. Firstly, the algorithm is fed with the ratio of subtracted volume to total volume, which approximates the ratio of subtracted weight.

$$V_{target} = V_{orig} \times (1 - R) \tag{2.1}$$

Scaling Factors

In the realm of adipose distribution, individual variance is substantial and intricately intertwined with factors such as age, gender, race, and Body Mass Index (BMI). For instance, while certain patients may exhibit a pronounced concentration of adiposity within the abdominal region, others might predominantly display it in areas like the hips and thighs. Such disparities in fat distribution patterns play a pivotal role in determining the magnitude of the reduction factor corresponding to each anatomical site during weight loss simulations.

The present algorithm empowers researchers to adjust the proportionality factor in concordance with the patient's unique physiological and adipose profile. Consequently, the resultant simulations more accurately mirror the post-weight-loss morphology of the patient in question. Such a personalized approach underscores the importance of catering to individual differences, ensuring that the outcomes of the algorithm are not merely generic, but a closer representation of the realistic post-operative or post-weight-loss scenario for each individual.

Iterative Method

The iterative method we're using is essentially a feedback control loop where we adjust the scale of the armature and then measure the volume of the resultant shape to see if it matches the target volume. Given this understanding, the mathematical representation can be described as follows:

Let's denote:

V_{orig} as the original volume. V_{target} as the desired target volume after weight loss. $V_{current}$ as the volume at the current iteration. SF_{bone} as the scale factor associated with a specific bone. T_{bone} as the tolerance associated with a specific bone. n as the number of iterations.

To reduce $V_{current}$ iteratively to approach V_{target}. The scale adjustment in each iteration for a specific bone is:

$$SF_{bone,new} = SF_{bone,old} - T_{bone} \tag{2.2}$$

Where $SF_{bone,old}$ is the scale factor of the bone from the previous iteration, and $SF_{bone,new}$is the updated scale factor for the current iteration.

The iterative process can be formally defined as:

$$V_{current,new} = V_{current,old} \times \prod_{i=1}^{N} SF_{bone,new}^{(i)} \tag{2.3}$$

Where N is the number of bones being adjusted.

The loop's termination criteria are:

$$|V_{current} - V_{target}| < \varepsilon \tag{2.4}$$

Where ε is a very small value indicating how close the current volume is to the target volume.

This iterative loop can be encapsulated in a function:

$$\begin{cases} V_{orig} & if\ n = 0 \\ V_{current}(n-1) \times \prod_{i=1}^{N} SF_{bone}^{(i)}(n) & otherwise \end{cases} \tag{2.5}$$

Where $SF_{bone}^{(i)}(n) = SF_{bone}^{(i)}(n-1) - T_{bone}^{(i)}$ for each i.

This mathematical representation encapsulates the core iterative methodology of my algorithm, adjusting scale factors based on tolerances and measuring resultant volume changes until convergence is achieved.

Outputs

Upon execution, the algorithm culminates in the generation of a refined body mesh, delineating the front-back and left-right scaled reductions for each anatomi-

cal section, with the height remaining unchanged. This output not only presents a quantified overview of the percentage reductions corresponding to each segment but also establishes a foundational platform for the ensuing modelling phases, particularly in the intricate simulation of skin folds post-weight reduction. This algorithm ensures that the resultant simulations are grounded in empirical data, thereby bolstering the precision and relevance of the subsequent morphological transformations within the context of post-operative or post-weight-loss scenarios.

2.2.3 Skin Fold Areas

From an extensive review of the existing literature, it has been elucidated that specific anatomical regions are predisposed to the manifestation of skin folds or sagging post-significant weight reduction. Notably, these regions encompass the abdomen, arms, thighs, and uniquely in females, the mammary glands.

Given the vast individual differences in anatomy and fat distribution, it becomes imperative to customize the simulation to cater to the unique physiological characteristics of each patient. As such, prior to the algorithmic simulation, an essential preparatory phase involves the meticulous demarcation of potential skin fold regions on the initial 3D model(Fig.2.6). This task mandates seasoned expertise in weight loss dynamics and an understanding of post-operative skin responses.

Leveraging Blender's versatile capabilities, this demarcation process is seamlessly executed using its intrinsic 'draw weights' functionality. This tool facilitates the delineation of specific regions that are hypothesized to undergo sagging or folding post-weight loss. It's pivotal to underscore that only these specifically demarcated zones are subjected to the dynamic skin fold simulation in the subsequent stages of the algorithm. The remaining portions of the model, deemed to remain anatomically invariant, are deliberately kept stationary to uphold the integrity and realism of the simulation.

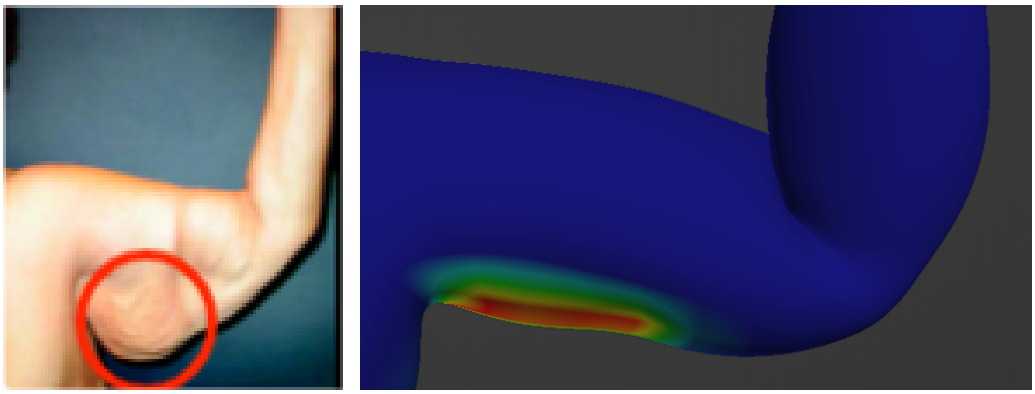

(a) Actual Skin Fold Area (red circle)

(b) Draw the Skin Fold Area (the degree of red represents the degree of skin fold)

Figure 2.6: Skin Fold Areas(eg: Left Upper Arm)

2.2.4 Skin Folds Simulation Algorithm

This secondary algorithm taps into Blender's clothing simulation capabilities, rooted in the mass-spring model. It serves to emulate the onset of skin folds and sagging that commonly follows substantial weight loss.

Mass-Spring Model(MSM)

The MSM has evolved as a staple tool in the fields of computational biomechanics and graphics, offering a robust framework for simulating the dynamic behaviour of deformable entities such as skin. By considering the skin as a composite of discrete mass nodes connected via springs, the MSM can replicate various mechanical behaviours based on the elasticity and force interactions among these springs and masses.

Mathematically, the behavior of each spring-mass node in the MSM is governed by Newton's second law:

$$F_{gravity} = m \times g \tag{2.6}$$

Where:

$F_{gravity}$ is the total force applied to a specific skin node. m represents the nodal mass. g is the acceleration due to gravity, typically $9.81 m/s^2$ on the surface of the Earth.

Additionally, the spring force, F_{spring}, influencing each node is derived from

Hooke's law:

$$F_{spring} = -k \times \Delta x \tag{2.7}$$

Where:

k stands for the spring's elastic modulus, indicative of the skin's inherent elasticity. Δx embodies the deviation from the spring's or skin node's rest position.

For the targeted simulation of skin folds, the subsequent forces are of utmost significance:

Tensional Force: Resembles the skin's resistance when being stretched.

$$F_{tension} = k_{tension} \times \Delta x \tag{2.8}$$

Compressional Force: Mirrors the skin's counteraction against compressive forces.

$$F_{compression} = k_{compression} \times \Delta x \tag{2.9}$$

Bend Force: Replicates the skin's resistance against changes in its curvature.

$$F_{bending} = k_{bending} \times \Delta \theta \tag{2.10}$$

Where $\Delta\theta$ quantifies the change in curvature angle of the skin.

Shear Force: Represents the skin's response to lateral strains.

$$F_{shear} = k_{shear} \times \Delta x \tag{2.11}$$

The algorithm commences with a manual demarcation of potential skin fold areas on a mesh. Once identified, these areas, categorized under the 'Fold' vertex group, undergo spatial manipulations based on assigned weight parameters, emulating the skin's post-weight loss response.

To engender a realistic simulation, the cloth physics system rooted in the MSM is employed. By intricately setting the system's stiffness coefficients—tension, compression, bending, and shear—the model aptly simulates post-operative skin fold dynamics.

Graded Skin Folds Simulation

A crucial consideration in the modelling process is the inherent variability of skin folds in patients post-weight loss. It is widely recognized that skin fold levels differ substantially among individuals, based on factors such as genetics, age, the duration of being overweight, and the rapidity of weight loss. To account for this unpredictability, the algorithm is devised to generate a range of possible outcomes rather than a singular deterministic result.

Outputs

Upon executing the algorithm, a series of models representing varying degrees of skin fold presence is generated. These models range from the least to the most pronounced skin folds. Each rendition is then presented to the patient, offering a comprehensive visual spectrum of potential postoperative outcomes. By encompassing the extremities of possible skin behaviours, this approach ensures patients receive a holistic visualization, fostering an informed perspective on the diverse possibilities concerning post-surgical skin appearance. This not only aids in setting realistic expectations but also equips the patient with a tangible understanding, further enhancing the decision-making process related to potential interventions.

2.3 VR Application

2.3.1 VR Scenes

To provide an immersive and tangible representation of post-surgical body transformations, particularly focusing on changes in body shape and skin folds, specific VR environments were crafted using Unity(2022.3.5f1). These VR scenarios give patients an intimate understanding of their post-operative physiques in various everyday contexts.

Swimming Pool Scene

This scene illustrated a quintessential family pool setting, characterized by pristine blue waters, a tiled pool bottom, and a diving platform(Fig.2.7). Considering that a family pool is a common environment where individuals often grapple with body image concerns, this setting was specifically chosen to aid patients in visualizing their post-surgical bodies in a casual, familiar space. Navigating through this

VR pool setting allowed patients to envisage potential future interactions, thereby building their confidence and assuaging any apprehensions about showcasing their transformed bodies during family pool outings.

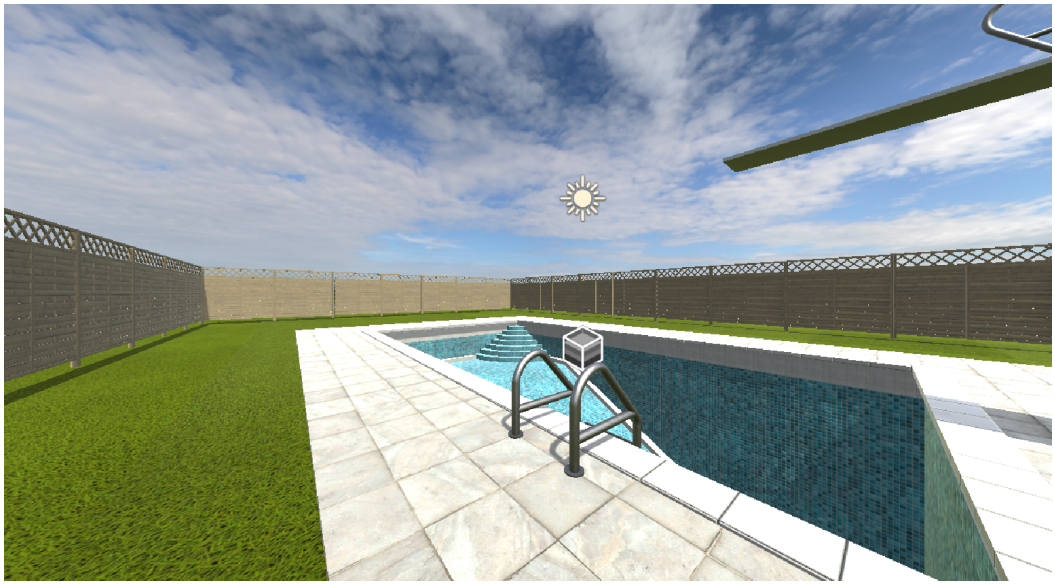

Figure 2.7: Swimming Pool Scene

Beach Scene

Mimicking a tranquil beachfront, the scene showcased golden sands, gently lapping waves and tropical trees(Fig.2.8). The beach, often a place of heightened body consciousness, served as a pertinent backdrop for patients to evaluate their comfort levels with their post-surgical physiques in swimwear. Engaging with this VR beach setting gave patients an opportunity to gauge their self-assurance and readiness for beach outings post-operation.

Figure 2.8: Beach Scene

Cloakroom Scene

Designed to mirror a standard cloakroom or changing facility, it was adorned with lockers, benches, and soft overhead lighting(Fig.2.9). Cloakrooms, as semi-public settings, often become places of inadvertent body comparisons. This environment was thus chosen to understand patients' comfort and confidence levels in such enclosed spaces. Immersion in this scene was intended to help patients assess their feelings in situations where changing clothes in semi-public settings is requisite, aiming to understand their level of self-acceptance in their new physical state.

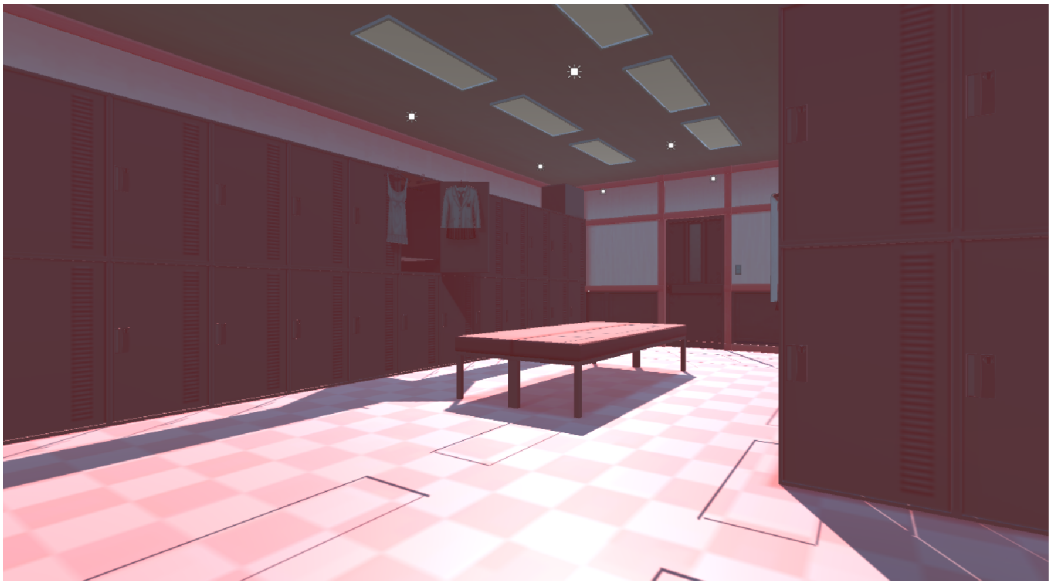

Figure 2.9: Cloakroom Scene

In summary, each VR environment, meticulously detailed and representative of everyday scenarios, served as an invaluable tool. They enabled patients to foresee, understand, and mentally prepare for their experiences and interactions in their newly transformed bodies.

2.3.2 VR Configuration

Upon the successful 3D reconstruction of each patient's physique, the models were imported into Unity from Blender, setting the stage for immersive visualization. To facilitate a seamless transition to the Oculus Quest 2 VR headset (Meta Platforms Inc, California, USA)(Fig.2.10), we harnessed the capabilities of a proprietary Oculus plug-in within Unity. This integration was pivotal for our primary objective: to offer patients a multi-perspective, immersive experience of their post-operative simulated bodies within the bespoke VR scenarios.

Figure 2.10: Oculus Quest 2 VR Headset and Hand Controllers

Third-Person Perspective

The third-person viewpoint was realized using the 'player control' prefab available in the Oculus plug-in.

This perspective empowered patients with the freedom to navigate the VR environment using Oculus controllers. Simultaneously, they could observe their simulated post-operative avatar manoeuvring through the scene.

The third-person view serves as an external observer perspective, allowing patients to critically analyze their post-surgical simulations in the context of the en-

vironment. This detached viewpoint offers a reflective space where patients can engage in a comparative analysis between their current physical state and the anticipated outcome.

First-Person Perspective

To achieve a first-person viewpoint, both the 'camera' and 'player control' prefabs within the Oculus plug-in were employed. The camera was meticulously bound to the avatar's head, ensuring that the patients' gaze in the VR mirrored the viewpoint of their reconstructed model.

Patients can use Oculus controllers to synchronize the movement of their avatars and their positioning within the VR environment.

The first-person perspective delivers an immersive and personalized experience, letting patients perceive their surroundings and their new physical state from their own vantage point. This perspective not only offers a subjective view of the changes but also engenders a deeper emotional and psychological connection, facilitating a more profound understanding of their post-operative transformations in relation to their environment.

In essence, the dual-perspective approach was strategically employed to cater to two distinct cognitive needs: one for objective analysis and another for immersive self-association. This duality ensures a holistic and comprehensive engagement with the post-surgical simulations, fostering both intellectual understanding and emotional acceptance.

Chapter 3

Results

3.1 3D Scanning

To evaluate the precision of the three scanning techniques mentioned in methodology session - the 1-minute flat scan, 2.5-minute flat scan, and the 2.5-minute up and down scan- a static human head stereo model was employed as a standard benchmark. This static model offers the advantage of remaining stationary, thereby facilitating a more consistent comparison across scanning methods. Utilizing a straightedge, a series of facial feature dimensions were directly measured on the model(Fig.3.1). These measurements encompassed the distance between midpoints of the left and right eyebrows (D1), the interocular distance (D2), distances from the left and right eyes to their respective eyebrows (D3 and D4), lengths of the left and right eyes (D5 and D6), distance from the nasal tip to the mouth (D7), from the mouth to the mandible tip (D8), and the overall mouth length (D9)(Fig.3.2). For the 3D models acquired through scanning, these facial dimensions were ascertained using the Rhino 7 3D industrial design software(Fig.3.3). Discrepancies between the real and 3D scanned measurements were subsequently determined(Table.3.1).

To represent the discrepancy between the true measurements and the ones derived from the 3D scanning techniques, the Mean Absolute Error (MAE) was computed for each scanning method.

$$MAE = \frac{1}{n}\sum_{i=1}^{n}|y_i - \hat{y}_i| \tag{3.1}$$

where y_i represents the true measurements, $\hat{y}_i$ denotes the corresponding measurements from the 3D scans, and n is the total number of measurements.

Table 3.1: Comparison of Eigenvalue Positions between Actual and Scanned Measurements

Feature	Actual (cm)	1-min Diff. (cm)	2.5-min Flat Diff. (cm)	2.5-min Up/Down Diff. (cm)
D1	80.1	-2.4	-0.9	+0.3
D2	85.9	-5,2	-5.0	-5.0
D3	29.0	-3.0	+0.2	-1.0
D4	26.5	-2.5	-3.0	+0.2
D5	33.1	-2.6	-2.0	-1.5
D6	30.0	-2.0	+2.7	-2.3
D7	28.5	-4.2	-3.0	-2.9
D8	55.0	+1.5	-0.7	+0.6
D9	65.0	-7.6	-4.1	-4.5

37

Figure 3.1: Actual Measurements

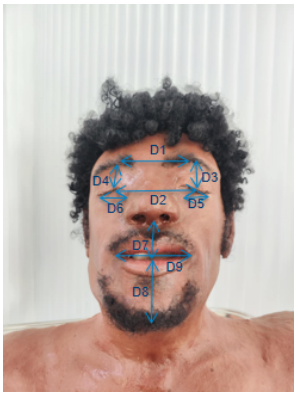

Figure 3.2: Facial Eigenvalue

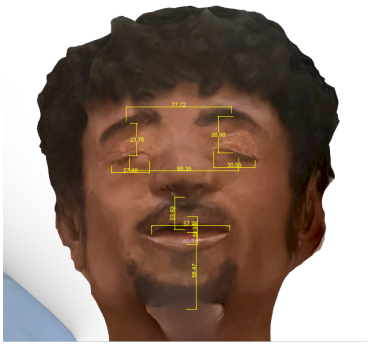

Figure 3.3: 3D Scanning Model Measurements(eg: 1-min flat)

- **1-minute flat scan:** MAE = 3.4
- **2.5-minute flat scan:** MAE = 2.4
- **2.5-minute up and down scan:** MAE = 2.0

The results denote a clear trend of increasing accuracy with prolonged scan duration and the incorporation of varied scanning angles. Specifically, the 2.5-minute up and down scan displayed the lowest MAE value of 2.0, making it the most precise among the evaluated methods. However, while it outperforms the 1-minute flat scan by a significant margin, its advantage over the 2.5-minute flat scan, which has a slightly higher MAE of 2.4, is less pronounced. This indicates that while duration plays a role in the accuracy, the scanning pattern (up and down motion) appears to also contribute to the refined precision.

3.2 3D Reconstruction

The results pertaining to the 3D reconstruction process are bifurcated into two distinct phases: the preliminary stage of body size reduction, followed by the subsequent phase of skin fold simulation. This structured presentation allows for a coherent understanding of the transformational journey, from the initial body representation to the final post-operative simulated reconstruction.

3.2.1 Body Size Reduction

Our analysis leveraged anthropometric data sourced from the Ankit et al study[62], which tracked patients post their bariatric surgery interventions. Through this detailed dataset, we ascertained the proportionate reductions across distinct body

regions. These measurements subsequently informed the scale factor allocations for each segment of the armature. Proceeding from the initial model, a sequence of body representations was devised, capturing the gradual weight loss journey up to 30%, in consistent 5% intervals(Fig.3.4, Fig.3.5). A salient note is that the conceptualization of 'weight reduction' in this context aligns with a diminution in the model grid's volumetric parameters. The tabulated data below delineates the scale factors concurrent with the percentage reductions for each segmentation of illustrative models(Table.3.2).

(a) Original (b) 5% WL (c) 10% WL (d) 15% WL (e) 20% WL (f) 25% WL (g) 30% WL

Figure 3.4: Trends in body size reduction (Front View)

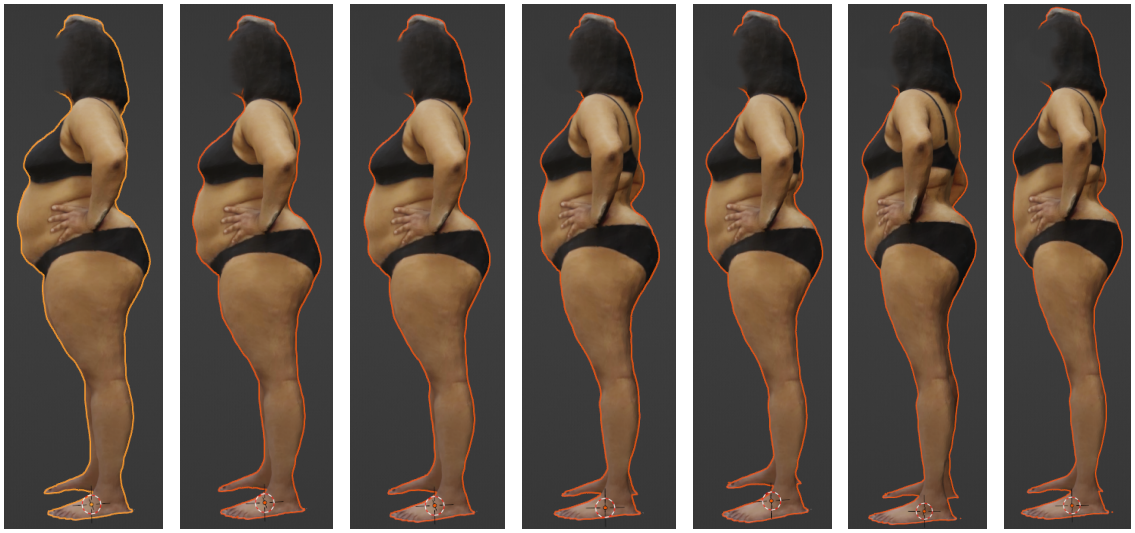

(a) Original (b) 5% WL (c) 10% WL (d) 15% WL (e) 20% WL (f) 25% WL (g) 30% WL

Figure 3.5: Trends in body size reduction (Side View)

3.2.2 Skin Fold Simulation

In our analysis, the methodology for simulating skinfolds was informed by the grading criteria established for post-bariatric surgery body contour deformities, as

Table 3.2: Scale Factors and Percentage Reductions for Each Model

Body Part	**Tolerance**	**% Reduction at 5% WL**	**10% WL**	**15% WL**	**20% WL**	**25% WL**	**30% WL**
Head	0.039	1.4	2.7	4.4	5.7	7.6	9.1
Neck	0.143	5.1	9.9	16.0	21.0	27.7	33.3
Chest	0.178	6.4	12.3	19.9	26.2	34.5	41.5
Abdomen	0.205	7.4	14.1	23.0	30.1	39.8	47.8
Pelvis	0.228	8.2	15.7	25.5	33.5	44.2	53.1
Buttock	0.228	8.2	15.7	25.5	33.5	44.2	53.1
Left Upper Arm	0.156	5.6	10.8	17.5	22.9	30.3	36.3
Right Upper Arm	0.156	5.6	10.8	17.5	22.9	30.3	36.3
Left Forearm	0.078	2.8	5.4	8.7	11.5	15.1	18.2
Right Forearm	0.078	2.8	5.4	8.7	11.5	15.1	18.2
Left Hand	0.039	1.4	2.7	4.4	5.7	7.6	9.1
Right Hand	0.039	1.4	2.7	4.4	5.7	7.6	9.1
Left Thigh	0.156	5.6	10.8	17.5	22.9	30.3	36.3
Left Calf	0.078	2.8	5.4	8.7	11.5	15.1	18.2
Left Foot	0.039	1.4	2.7	4.4	5.7	7.6	9.1
Right Thigh	0.156	5.6	10.8	17.5	22.9	30.3	36.3
Right Calf	0.078	2.8	5.4	8.7	11.5	15.1	18.2
Right Foot	0.039	1.4	2.7	4.4	5.7	7.6	9.1

outlined in the research by Martin et al[60]. We commenced by focusing on predominant areas of deformity, notably the abdomen, arms, thighs, and mammary glands (in females). Subsequent sections provide a detailed representation of skin-fold simulations corresponding to each grade for the aforementioned regions. To culminate, a comprehensive depiction of the overall skin deformity is provided. For illustrative purposes, we opted for a model with a higher degree of obesity to vividly demonstrate the impact of varying skin fold levels.

Arms

During our simulation, the arm was positioned in abduction(Fig.3.6). Within its middle third, we defined the amplitude of the arm, spanning from the upper to the lower boundary of the muscle mass, discernible upon palpation. A standard amplitude was categorized as 100%. Grading was determined based on increments of 50% relative to this arm amplitude(Fig.3.7):

Grade 1: The skin flap extends beyond the standard, covering up to an additional 50% of the arm amplitude.

Grade 2: The skin flap's projection lies between 50% and 100% of the designated arm amplitude.

Grade 3: The skin flap's extension surpasses the standard, ranging between 100% and 150% of the arm amplitude.

Grade 4: The skin flap demonstrates a pronounced extension, ranging from 150% to 200% of the original arm amplitude.

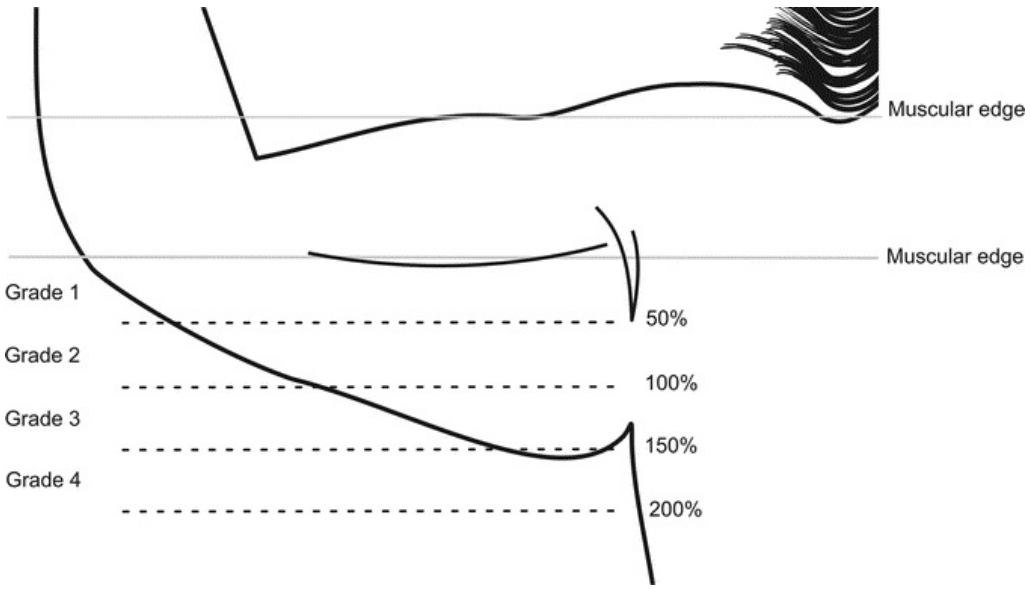

Figure 3.6: Skin fold grading of the arm (Example)

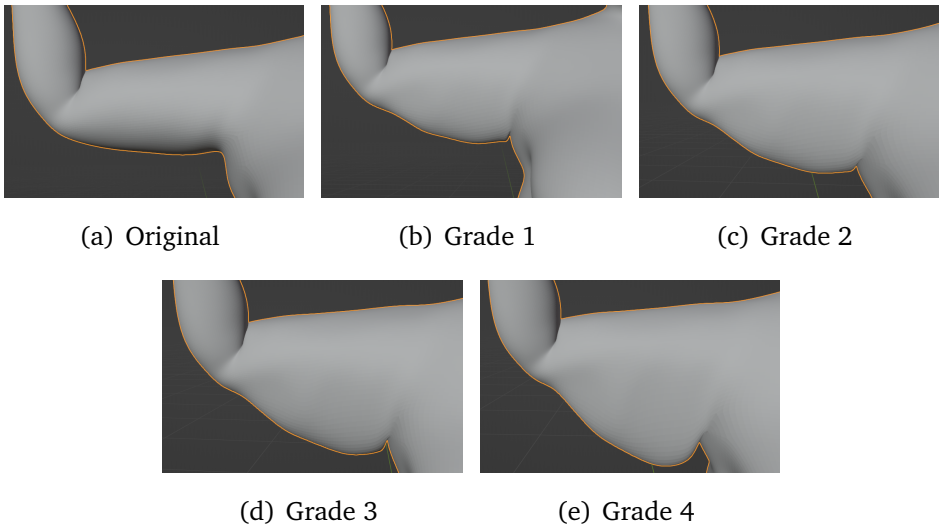

(a) Original (b) Grade 1 (c) Grade 2

(d) Grade 3 (e) Grade 4

Figure 3.7: Arm skin fold simulation grading

Thighs

For the assessment of the thighs, the leg was positioned in both flexion and abduction(Fig.3.8). Within the middle third of the thigh, the total amplitude was demarcated, stretching from the upper to the lower boundary of the muscular mass, discernible upon palpation. Grading criteria were set based on increments of 50% relative to this thigh amplitude(Fig.3.9):

Grade 1: The skin flap extends beyond the baseline, encompassing up to an additional 50% of the thigh amplitude.

Grade 2: The projection of the skin flap lies between 50% and 100% of the pre-determined thigh amplitude.

Grade 3: The extension of the skin flap surpasses the baseline, ranging between 100% and 150% of the thigh amplitude.

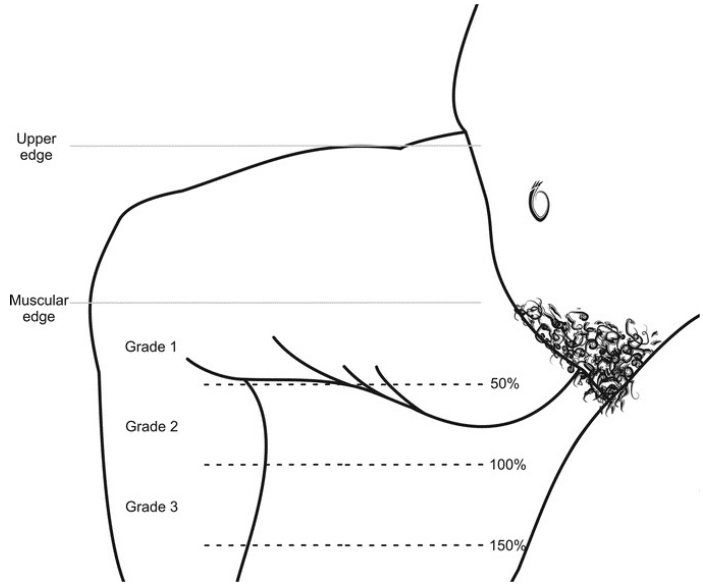

Figure 3.8: Skin fold grading of the thigh (Example)

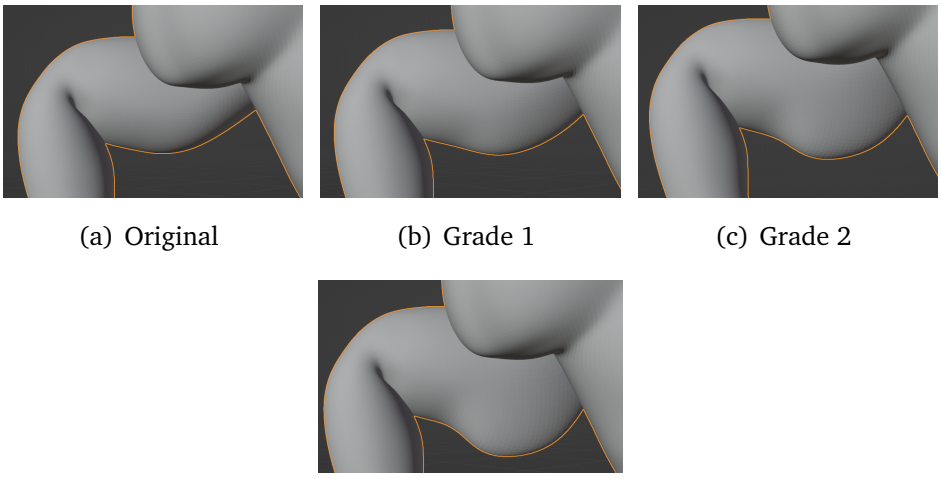

(a) Original (b) Grade 1 (c) Grade 2

(d) Grade 3

Figure 3.9: Thigh skin fold simulation grading

Abdomen

For the abdominal region, the evaluation focuses on the extent of the redundant pannus in relation to specific anatomical landmarks, notably the inguinal ligament and the entire span of the thigh(Fig.3.10). The thigh's length was subdivided into three distinct segments: the upper, middle, and lower thirds. Based on this stratification, the following grading system was implemented to classify the pannus' extent(Fig.3.11):

Grade 1: The pannus remains positioned exclusively above the level of the inguinal ligament.

Grade 2: The descent of the pannus surpasses the inguinal ligament without extending beyond the upper third boundary of the thigh.

Grade 3: The pannus' projection is situated within the confines of the thigh's middle third.

Grade 4: The overhanging pannus reaches down into the thigh's lower third segment.

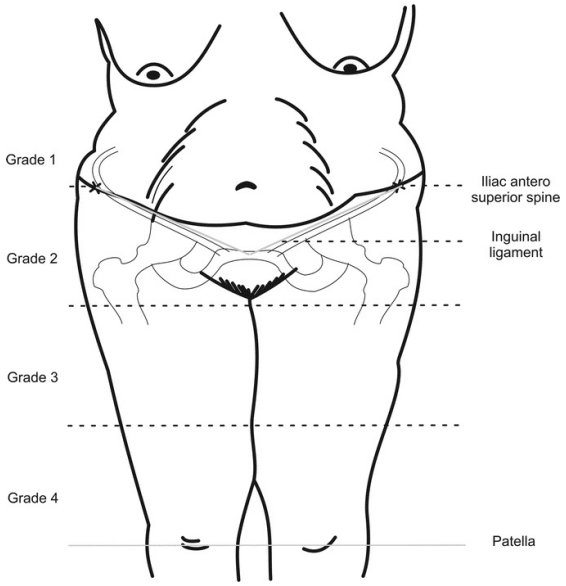

Figure 3.10: Skin fold grading of the abdomen (Example)

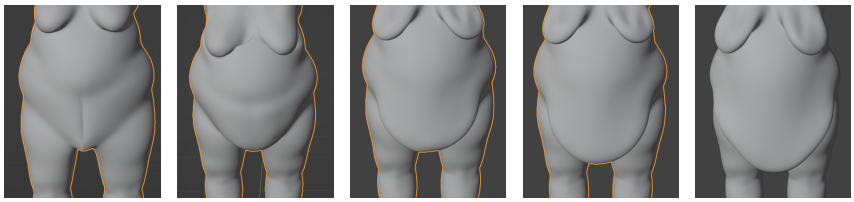

(a) Original (b) Grade 1 (c) Grade 2 (d) Grade 3 (e) Grade 4

Figure 3.11: Abdomen skin fold simulation grading

Mammary Gland (Female)

For the assessment of the mammary gland, the inframammary fold, typically aligned with the sixth rib, serves as the proximal benchmark(Fig.3.12). Conversely, the upper boundary of the ipsilateral iliac crest is employed as the distal point of reference. The span between these two anatomical landmarks is systematically segmented into the upper, middle, and lower thirds. The grading system was subsequently developed based on the positioning of the breast's inferior edge relative to these delineated thirds(Fig.3.13, Fig.3.14):

Grade 1: The inferior boundary of the mammary gland remains within the confines of the upper third.

Grade 2: The breast's lower margin is situated within the middle third region.

Grade 3: The termination of the breast descends into the lower third segment.

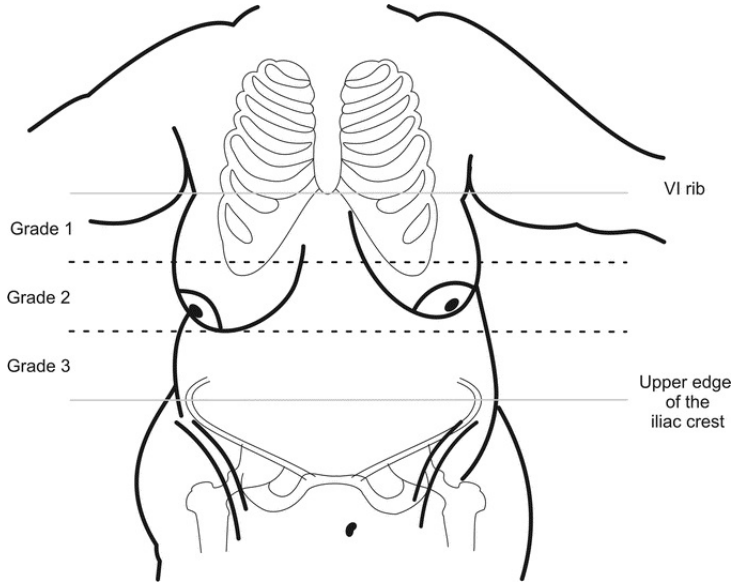

Figure 3.12: Skin fold grading of the Mammary Gland (Example)

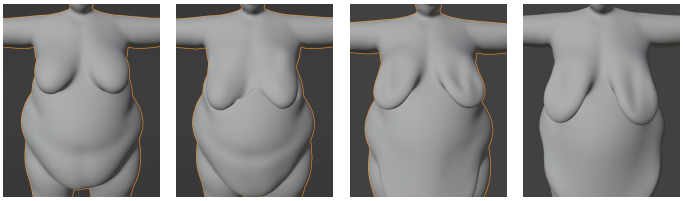

(a) Original (b) Grade 1 (c) Grade 2 (d) Grade 3

Figure 3.13: Mammary gland skin fold simulation grading (Front View)

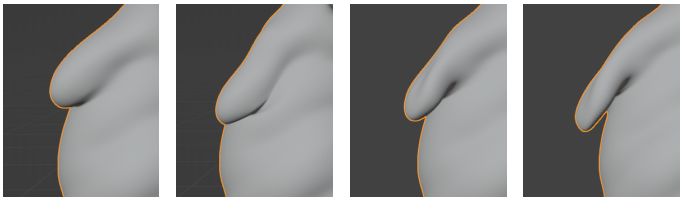

(a) Original (b) Grade 1 (c) Grade 2 (d) Grade 3

Figure 3.14: Mammary gland skin fold simulation grading (Side View)

3.2.3 Whole Body Simulation

Upon the execution of body size diminution and skin fold simulation, resultant imagery depicting the post-weight loss physique was generated. Within this segment of results, visual representations of the scanned model are showcased, encapsulating the simulation of a mildly obese female subjected to weight reductions of 15% and 25%. For the purposes of this illustration, a consistent skin deformity grade of 1 was attributed across all anatomical sections(Fig.3.15).

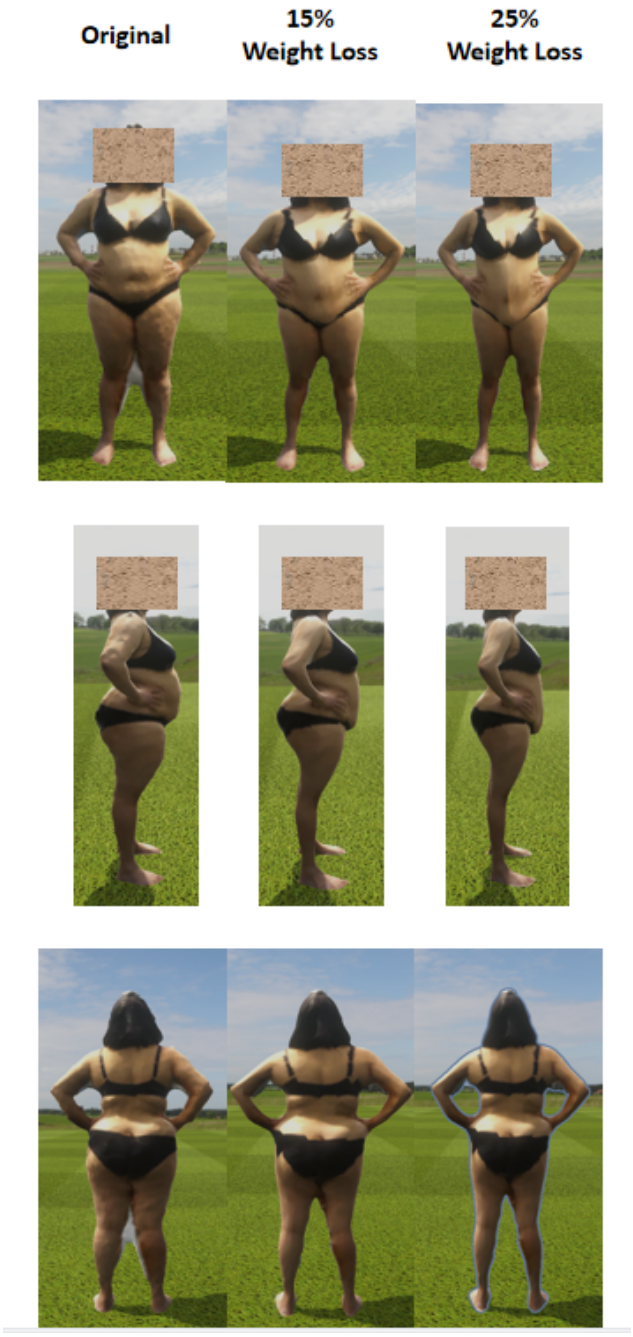

Figure 3.15: Whole Body Simulation

Furthermore, real scan models were reconstructed based on data generously provided by Nazrin[61]. These reconstructions vividly illustrate significant reductions in body mass, specifically in the arms, thighs, and abdomen of each participant. For Participants 1(Fig.3.16), 2(Fig.3.17), 4(Fig.3.19), and 6(Fig.3.21), who exhibited milder levels of obesity, a Level 1 skin fold effect was applied to approximate the anticipated skin changes post-weight loss. In the case of Participant 5(Fig.3.20), who displayed a more elevated level of obesity relative to the others, a Level 2 skin fold effect was employed. Most notably, Participant 3(Fig.3.18), who had the highest obesity level among all participants, was modelled with a Level 3 skin fold effect to accurately represent his projected post-surgical skin laxity.

(a) Original (b) 25% WL (c) Original (d) 25% WL

Figure 3.16: Original model and post-bariatric surgery simulation model for Participant 1

(a) Original (b) 25% WL (c) Original (d) 25% WL

Figure 3.17: Original model and post-bariatric surgery simulation model for Participant 2

(a) Original (b) 25% WL (c) Original (d) 25% WL

Figure 3.18: Original model and post-bariatric surgery simulation model for Participant 3

(a) Original (b) 25% WL (c) Original (d) 25% WL

Figure 3.19: Original model and post-bariatric surgery simulation model for Participant 4

(a) Original (b) 25% WL (c) Original (d) 25% WL

Figure 3.20: Original model and post-bariatric surgery simulation model for Participant 5

(a) Original (b) 25% WL (c) Original (d) 25% WL

Figure 3.21: Original model and post-bariatric surgery simulation model for Participant 6

3.3 VR Applications

Upon successful acquisition of the reconstructed imagery, it was subsequently imported into the Unity platform. Within this digital framework, the reconstructed depiction was configured to align with distinct virtual landscapes. These simulated environments encompassed a beach setting(Fig.3.26, Fig.3.27), a swimming pool tableau(Fig.3.22, Fig.3.23), and a cloakroom scenario(Fig.3.24, Fig.3.25). Post-alignment of the reconstructed avatar with these immersive scenes, both first-person and third-person viewpoints were calibrated for optimal user experience. Conclusively, the entirety of this project was transferred to the Oculus Quest 2 headset. Engaging with this state-of-the-art apparatus, participants were endowed with a virtual glimpse into their prospective physiques post-weight reduction.

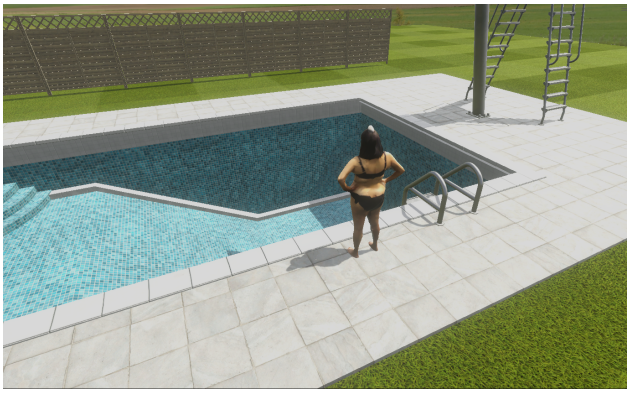

Figure 3.22: Swimming Pool Scenario Third View

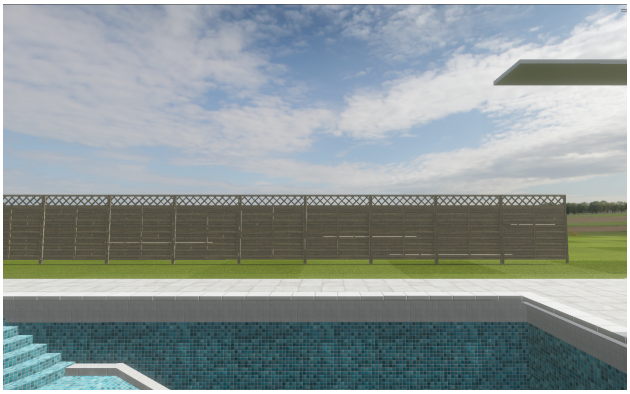

Figure 3.23: Swimming Pool Scenario First View

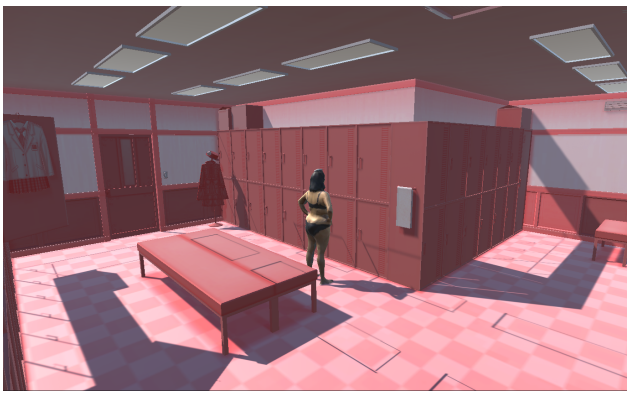

Figure 3.24: Cloakroom Scenario Third View

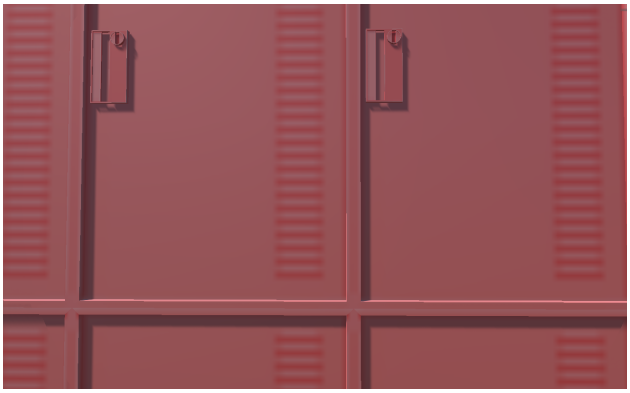

Figure 3.25: Cloakroom Scenario First View

Figure 3.26: Beach Scenario Third View

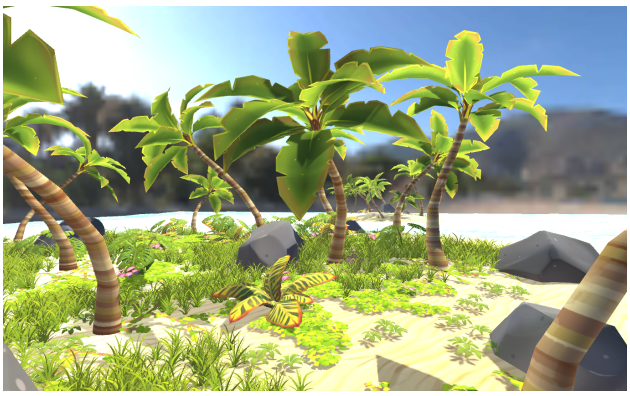

Figure 3.27: Beach Scenario First View

Chapter 4

Discussion

4.1 Conclusion and Achievements

In the realm of 3D scanning, the current study embarked on a quantitative exploration into the implications of varying scanning durations and trajectories on the fidelity of the generated models. It provides a reference for the selection of relevant experimental scanning methods in the future.

As we ventured into the intricacies of 3D reconstruction, this research introduced two pioneering algorithms, hallmarked by their tailored simplicity and efficient coding paradigms. The first, an armature iterative algorithm, facilitates the meticulous modulation of individual body segment volumes, reflecting distinct weight loss percentages. Contrary to prevailing methodologies which homogenously equate overall volume reduction to weight loss, this algorithm acknowledges the idiosyncratic weight loss patterns of post-bariatric interventions. It is instrumental in discerning differential weight reductions across regions, such as the more pronounced loss in the abdomen relative to extremities like hands. The subsequent algorithm delves into skin fold simulation. By adeptly harnessing the principles of the mass-spring model in physics, it emulates the sagging of skin, reminiscent of a spring under gravity, post substantive weight loss. Traditional approaches, reliant on intricate sculpting techniques, demand extensive time commitments and significant expertise in model manipulation. This novel algorithm, however, culminates in a sixfold reduction in modeling time, simplifying the process considerably. Additionally, a contribution of this research lies in its presentation of graded renderings that elucidate skin deformities post-bariatric surgery. These delineated depictions serve for future studies in this domain.

Navigating towards virtual reality applications, previous scholarly endeavours

predominantly employed a third-person perspective, relegating participants to mere observers of their post-weight loss transformation. Breaking new ground, our study integrated an immersive first-person perspective, fostering a profound sense of embodiment. This innovation empowers participants to not only visually appreciate their post-operative transformation but also to viscerally experience their new self within a virtual environment.

4.2 Limitation

From a hardware standpoint, our research utilized a commonplace handheld tablet for scanning purposes. Although convenient, this tablet, with its inherent LiDAR scanning capabilities, pales in comparison to the precision offered by professional-grade scanning apparatuses. Notably, the scans captured exhibited imperfections, particularly in intricate regions such as fingertips, hair strands, and earlobes. Such inconsistencies invariably introduce discrepancies into the final simulation model, potentially detracting from the patient's virtual experience.

In relation to the software employed, while Blender3D stands as a formidable tool in the domain of modeling, it isn't devoid of shortcomings. Though the mesh was intricately reconstructed, a holistic model mandates seamless integration of mesh and texture. Concurrent reconstruction of both proves challenging, leading to sporadic misalignments. This was evident in instances of facial feature deformities, discontinuities in textures like underwear, and similar nuances, which inadvertently compromise the user experience.

Regarding the algorithmic framework, the current iteration does not provide a stand-alone, fully automated solution. Firstly, Blender serves as an indispensable intermediary for code execution. Additionally, it mandates researchers to possess a foundational understanding of bariatric procedures. This knowledge is instrumental in facilitating personalized pre-processing stages, which encompass tasks such as aligning bones with the mesh or demarcating skin fold regions.

Lastly, the validation phase of the study was met with its own set of challenges. Ethical considerations and time constraints rendered it untenable to onboard a vast patient cohort for extensive testing and subsequent follow-ups. As a consequence, the assessment of simulation authenticity currently rests upon the subjective visual evaluations of expert reviewers.

4.3 Future Work

The foundation laid by this study opens myriad avenues for advancement in subsequent research endeavors. There is evident potential in utilizing superior scanning tools to garner intricate details of the human physique, thus enhancing the accuracy of initial human appearance captures. Furthermore, the development of an intuitive visual interface for the program could streamline user operations, making the process more accessible and user-friendly.

A richer database, supplemented with extensive raw data, paves the way for the incorporation of machine learning techniques. Such an approach could intricately analyze the disparities in pre- and post-weight loss human body presentations, culminating in refined simulation predictions. The validation phase could benefit immensely from insights offered by a broader spectrum of experts specializing in weight loss, ensuring a holistic evaluation and testing of the program.

With an extended research timeline, the opportunity arises to meticulously monitor the morphological transitions experienced by patients post-bariatric surgery. This, in turn, could refine and further optimize the existing program algorithms.

Bibliography

[1] W. H. Organization, "Obesity: preventing and managing the global epidemic: report of a who consultation," 2000.

[2] L. Abarca-Gómez, Z. A. Abdeen, Z. A. Hamid, N. M. Abu-Rmeileh, B. Acosta-Cazares, C. Acuin, R. J. Adams, W. Aekplakorn, K. Afsana, C. A. Aguilar-Salinas, *et al.*, "Worldwide trends in body-mass index, underweight, overweight, and obesity from 1975 to 2016: a pooled analysis of 2416 population-based measurement studies in 128· 9 million children, adolescents, and adults," *The lancet*, vol. 390, no. 10113, pp. 2627–2642, 2017.

[3] M. Ng, T. Fleming, M. Robinson, B. Thomson, N. Graetz, C. Margono, E. C. Mullany, S. Biryukov, C. Abbafati, S. F. Abera, *et al.*, "Global, regional, and national prevalence of overweight and obesity in children and adults during 1980–2013: a systematic analysis for the global burden of disease study 2013," *The lancet*, vol. 384, no. 9945, pp. 766–781, 2014.

[4] W. H. Organization *et al.*, "Obesity and overweight," 2017.

[5] E. A. Finkelstein, O. A. Khavjou, H. Thompson, J. G. Trogdon, L. Pan, B. Sherry, and W. Dietz, "Obesity and severe obesity forecasts through 2030," *American journal of preventive medicine*, vol. 42, no. 6, pp. 563–570, 2012.

[6] C. L. Ogden, S. Z. Yanovski, M. D. Carroll, and K. M. Flegal, "The epidemiology of obesity," *Gastroenterology*, vol. 132, no. 6, pp. 2087–2102, 2007.

[7] J. Wardle and D. Boniface, "Changes in the distributions of body mass index and waist circumference in english adults, 1993/1994 to 2002/2003," *International journal of obesity*, vol. 32, no. 3, pp. 527–532, 2008.

[8] M. of Health, "Tracking the obesity epidemic: New zealand 1977–2003," 2004.

[9] H. L. Walls, R. Wolfe, M. M. Haby, D. J. Magliano, M. De Courten, C. M. Reid, J. J. McNeil, J. Shaw, and A. Peeters, "Trends in bmi of urban australian

adults, 1980–2000," *Public health nutrition*, vol. 13, no. 5, pp. 631–638, 2010.

[10] G. . O. Collaborators, "Health effects of overweight and obesity in 195 countries over 25 years," *New England journal of medicine*, vol. 377, no. 1, pp. 13–27, 2017.

[11] Unicef, UNICEF, *et al.*, "Who-the world bank: Joint child malnutrition estimates-levels and trends," *World Health Organization, Geneva The World Bank, Washington, DC*, 2012.

[12] M. Agha and R. Agha, "The rising prevalence of obesity: part b—public health policy solutions," *International Journal of Surgery. Oncology*, vol. 2, no. 7, p. e19, 2017.

[13] M. Abdelaal, C. W. le Roux, and N. G. Docherty, "Morbidity and mortality associated with obesity," *Annals of translational medicine*, vol. 5, no. 7, 2017.

[14] J. O. Hill and J. C. Peters, "Environmental contributions to the obesity epidemic," *Science*, vol. 280, no. 5368, pp. 1371–1374, 1998.

[15] V. S. Malik, B. M. Popkin, G. A. Bray, J.-P. Després, and F. B. Hu, "Sugar-sweetened beverages, obesity, type 2 diabetes mellitus, and cardiovascular disease risk," *Circulation*, vol. 121, no. 11, pp. 1356–1364, 2010.

[16] B. M. Popkin, "Urbanization, lifestyle changes and the nutrition transition," *World development*, vol. 27, no. 11, pp. 1905–1916, 1999.

[17] Y. Raziani and S. Raziani, "Investigating the predictors of overweight and obesity in children," *Int. J. Adv. Stud. Humanit. Soc. Sci*, vol. 9, no. 4, pp. 262–280, 2020.

[18] R. J. Kuczmarski and K. M. Flegal, "Criteria for definition of overweight in transition: background and recommendations for the united states," *The American journal of clinical nutrition*, vol. 72, no. 5, pp. 1074–1081, 2000.

[19] ASMBS, "Estimate of bariatric surgery numbers, 2011-2020." Online, June 2022.

[20] M. Sundbom, "Laparoscopic revolution in bariatric surgery," *World journal of gastroenterology: WJG*, vol. 20, no. 41, p. 15135, 2014.

[21] W. J. Pories, "Bariatric surgery: risks and rewards," *The Journal of Clinical Endocrinology & Metabolism*, vol. 93, no. 11_supplement_1, pp. s89–s96, 2008.

[22] A. Aminian, S. Brethauer, J. Kirwan, S. Kashyap, B. Burguera, and P. Schauer, "How safe is metabolic/diabetes surgery?," *Diabetes, Obesity and Metabolism*, vol. 17, no. 2, pp. 198–201, 2015.

[23] A. A. Pona, R. J. Marek, L. J. Heinberg, M. Lavery, K. Ashton, and J. M. Rish, "Psychological correlates of body image dissatisfaction before and after bariatric surgery," *Bariatric Surgical Practice and Patient Care*, vol. 12, no. 4, pp. 184–189, 2017.

[24] A. J. Stunkard and T. A. Wadden, "Psychological aspects of severe obesity," *The American journal of clinical nutrition*, vol. 55, no. 2, pp. S524–S532, 1992.

[25] I. R. Knutsen, L. Terragni, and C. Foss, "Morbidly obese patients and lifestyle change: constructing ethical selves," *Nursing inquiry*, vol. 18, no. 4, pp. 348–358, 2011.

[26] R. M. Puhl and C. A. Heuer, "Obesity stigma: important considerations for public health," *American journal of public health*, vol. 100, no. 6, pp. 1019–1028, 2010.

[27] S. Lewis, S. L. Thomas, R. W. Blood, D. J. Castle, J. Hyde, and P. A. Komesaroff, "How do obese individuals perceive and respond to the different types of obesity stigma that they encounter in their daily lives? a qualitative study," *Social science & medicine*, vol. 73, no. 9, pp. 1349–1356, 2011.

[28] M. Meana and L. Ricciardi, *Obesity surgery: stories of altered lives*. University of Nevada Press, 2008.

[29] B. Christiansen, L. Borge, and M. Solveig Fagermoen, "Understanding everyday life of morbidly obese adults-habits and body image," *International journal of qualitative studies on health and well-being*, vol. 7, no. 1, p. 17255, 2012.

[30] M. Libeton, J. B. Dixon, C. Laurie, and P. E. O'brien, "Patient motivation for bariatric surgery: characteristics and impact on outcomes," *Obesity surgery*, vol. 14, no. 3, pp. 392–398, 2004.

[31] M. Roehrig, R. M. Masheb, M. A. White, B. S. Rothschild, C. H. Burke-Martindale, and C. M. Grilo, "Chronic dieting among extremely obese bariatric surgery candidates," *Obesity surgery*, vol. 19, pp. 1116–1123, 2009.

[32] L. M. Gibbons, D. B. Sarwer, C. E. Crerand, A. N. Fabricatore, R. H. Kuehnel, P. E. Lipschutz, S. E. Raper, N. N. Williams, and T. A. Wadden, "Previous

weight loss experiences of bariatric surgery candidates: how much have patients dieted prior to surgery?," *Surgery for Obesity and Related Diseases*, vol. 2, no. 2, pp. 159–164, 2006.

[33] J. Temple Newhook, D. Gregory, and L. Twells, "The road to "severe obesity": weight loss surgery candidates talk about their histories of weight gain," *Journal of Social, Behavioral, and Health Sciences*, vol. 7, no. 1, p. 3, 2013.

[34] J. Ogden, C. Clementi, and S. Aylwin, "The impact of obesity surgery and the paradox of control: A qualitative study," *Psychology & health*, vol. 21, no. 2, pp. 273–293, 2006.

[35] D. H. Sutton, N. Murphy, and D. A. Raines, "Transformation: The "life-changing" experience of women who undergo a surgical weight loss intervention," *Bariatric nursing and surgical patient care*, vol. 4, no. 4, pp. 299–306, 2009.

[36] L. E. Bocchieri, M. Meana, and B. L. Fisher, "Perceived psychosocial outcomes of gastric bypass surgery: a qualitative study," *Obesity surgery*, vol. 12, no. 6, pp. 781–788, 2002.

[37] J. Gilmartin, "Body image concerns amongst massive weight loss patients," *Journal of clinical nursing*, vol. 22, no. 9-10, pp. 1299–1309, 2013.

[38] J. I. Mechanick, A. Youdim, D. B. Jones, W. T. Garvey, D. L. Hurley, M. M. McMahon, L. J. Heinberg, R. Kushner, T. D. Adams, S. Shikora, *et al.*, "Clinical practice guidelines for the perioperative nutritional, metabolic, and nonsurgical support of the bariatric surgery patient—2013 update: cosponsored by american association of clinical endocrinologists, the obesity society, and american society for metabolic & bariatric surgery," *Surgery for Obesity and Related Diseases*, vol. 9, no. 2, pp. 159–191, 2013.

[39] S. Ramalho, A. P. Bastos, C. Silva, A. R. Vaz, I. Brandão, P. P. Machado, and E. Conceição, "Excessive skin and sexual function: relationship with psychological variables and weight regain in women after bariatric surgery," *Obesity surgery*, vol. 25, pp. 1149–1154, 2015.

[40] K. Lyons, B. A. Meisner, S. Sockalingam, and S. E. Cassin, "Body image after bariatric surgery: A qualitative study," *Bariatric surgical practice and patient care*, vol. 9, no. 1, pp. 41–49, 2014.

[41] A. U. Bauchowitz, L. A. Gonder-Frederick, M.-E. Olbrisch, L. Azarbad, M.-Y. Ryee, M. Woodson, A. Miller, and B. Schirmer, "Psychosocial evaluation of

bariatric surgery candidates: a survey of present practices," *Psychosomatic medicine*, vol. 67, no. 5, pp. 825–832, 2005.

[42] H. C. Henrickson, K. R. Ashton, A. K. Windover, and L. J. Heinberg, "Psychological considerations for bariatric surgery among older adults," *Obesity surgery*, vol. 19, pp. 211–216, 2009.

[43] J. Ogden, D. Ratcliffe, and V. Snowdon-Carr, "British obesity metabolic surgery society endorsed guidelines for psychological support pre-and post-bariatric surgery," *Clinical obesity*, vol. 9, no. 6, p. e12339, 2019.

[44] F. Mantovani, G. Castelnuovo, A. Gaggioli, and G. Riva, "Virtual reality training for health-care professionals," *CyberPsychology & Behavior*, vol. 6, no. 4, pp. 389–395, 2003.

[45] J. Dalton, M. Craven, A. Bergin, S. Ticho, R. O'Brien, I. Phelan, A. Carrion-Plaza, R. Price, A. Logeswaren, F. Kilkelly, *et al.*, "The growing value of xr in healthcare in the united kingdom," 2021.

[46] P. Cipresso, I. A. C. Giglioli, M. A. Raya, and G. Riva, "The past, present, and future of virtual and augmented reality research: a network and cluster analysis of the literature," *Frontiers in psychology*, p. 2086, 2018.

[47] G. L. Cesa, G. M. Manzoni, M. Bacchetta, G. Castelnuovo, S. Conti, A. Gaggioli, F. Mantovani, E. Molinari, G. Cárdenas-López, and G. Riva, "Virtual reality for enhancing the cognitive behavioral treatment of obesity with binge eating disorder: randomized controlled study with one-year follow-up," *Journal of medical Internet research*, vol. 15, no. 6, p. e113, 2013.

[48] A. Gendia, A. Zyada, M. T. Nasir, M. Elfar, M. Sakr, M. U. Rehman, A. Cota, J. Clark, M. K. Sakr, and M. U. REHMAN, "Virtual reality as a surgical care package for patients undergoing weight loss surgery: A narrative review of the impact of an emerging technology," *Cureus*, vol. 14, no. 9, 2022.

[49] B. Allen, B. Curless, and Z. Popović, "The space of human body shapes: reconstruction and parameterization from range scans," *ACM transactions on graphics (TOG)*, vol. 22, no. 3, pp. 587–594, 2003.

[50] E. ISO, "20685: 2019-01; 3-d scanning methodologies for internationally compatible anthropometric databases—part 1: Evaluation protocol for body dimensions extracted from 3-d body scans," *ISO: Geneva, Switzerland*, 2018.

[51] N. Koepke, M. Zwahlen, J. C. Wells, N. Bender, M. Henneberg, F. J. Rühli, and K. Staub, "Comparison of 3d laser-based photonic scans and manual

anthropometric measurements of body size and shape in a validation study of 123 young swiss men," *PeerJ*, vol. 5, p. e2980, 2017.

[52] J. Shan and C. Toth, *Topographic Laser Ranging and Scanning: Principles and Processing, Second Edition*. CRC Press, 2018.

[53] K. J. Ebeling, R. Michalzik, and H. Moench, "Vertical-cavity surface-emitting laser technology applications with focus on sensors and three-dimensional imaging," *Japanese Journal of Applied Physics*, vol. 57, 2018.

[54] H. Moench, S. Gronenborn, X. Gu, R. Gudde, M. Herper, J. Kolb, M. Miller, M. Smeets, and A. Weigl, "Vcsels in short-pulse operation for time-of-flight applications," in *Vertical-Cavity Surface-Emitting Lasers XXII*, vol. 10552, pp. 82–88, SPIE, 2018.

[55] W. Sun, Y. Hu, D. G. MacDonnell, C. Weimer, and R. R. Baize, "Technique to separate lidar signal and sunlight," *Optics express*, vol. 24, no. 12, pp. 12949–12954, 2016.

[56] M. S. Nielsen, B. J. Christensen, J. B. Schmidt, L. Tækker, L. Holm, S. Lunn, C. Ritz, N. J. Wewer Albrechtsen, J. J. Holst, T. M. Schnurr, *et al.*, "Predictors of weight loss after bariatric surgery—a cross-disciplinary approach combining physiological, social, and psychological measures," *International Journal of Obesity*, vol. 44, no. 11, pp. 2291–2302, 2020.

[57] D. Arterburn, R. Wellman, A. Emiliano, S. R. Smith, A. O. Odegaard, S. Murali, N. Williams, K. J. Coleman, A. Courcoulas, R. Y. Coley, *et al.*, "Comparative effectiveness and safety of bariatric procedures for weight loss: a pcornet cohort study," *Annals of internal medicine*, vol. 169, no. 11, pp. 741–750, 2018.

[58] A. Shah, M. Prasad, S. Devjani, P. Rai, M. Ashby-Thompson, W. W. Yu, D. Gallagher, and B. Laferrère, "Anthropometrics by three-dimensional photonic scanner in patients with obesity before and after bariatric surgery," *Obesity surgery*, vol. 31, pp. 53–61, 2021.

[59] A. Y. Song, R. D. Jean, D. J. Hurwitz, M. H. Fernstrom, J. A. Scott, and J. P. Rubin, "A classification of contour deformities after bariatric weight loss: the pittsburgh rating scale," *Plastic and reconstructive surgery*, vol. 116, no. 5, pp. 1535–1544, 2005.

[60] M. Iglesias, P. Butron, L. Abarca, M. F. Perez-Monzo, and B. de Rienzo-Madero, "An anthropometric classification of body contour deformities after

massive weight loss," *Annals of plastic surgery*, vol. 65, no. 2, pp. 129–134, 2010.

[61] N. Assaf, "The acceptability and feasibility of 3d reconstruction and virtual reality in addressing body image in bariatric surgery," 2022.

[62] A. Shah, M. Prasad, S. Devjani, P. Rai, M. Ashby-Thompson, W. W. Yu, D. Gallagher, and B. Laferrère, "Anthropometrics by three-dimensional photonic scanner in patients with obesity before and after bariatric surgery," *Obesity surgery*, vol. 31, pp. 53–61, 2021.

Appendix A

Armature Resizing Code

```
import bpy
import bmesh

def calculate_volume(mesh):
    bm = bmesh.new()
    bm.from_mesh(mesh)
    volume = bm.calc_volume()
    bm.free()
    return volume

def duplicate_mesh_and_calculate_volume(mesh, delete_mesh=
   True):
    mesh_copy = mesh.copy()
    mesh_copy.data = mesh_copy.data.copy()
    bpy.context.collection.objects.link(mesh_copy)
    mesh_copy.select_set(True)
    bpy.context.view_layer.objects.active = mesh_copy

    for modifier in mesh_copy.modifiers:
        if modifier.type == 'ARMATURE':
            bpy.ops.object.modifier_apply(modifier=modifier
               .name)

    volume = calculate_volume(mesh_copy.data)

    if delete_mesh:
        bpy.data.objects.remove(mesh_copy)
```

```
    return volume

def scale_bone_and_mesh(armature, bone_name, scale_factor,
   frame):
    bpy.context.view_layer.objects.active = armature
    bpy.ops.object.mode_set(mode='POSE')
    bone = armature.pose.bones[bone_name]
    bone.scale = scale_factor
    bone.keyframe_insert(data_path='scale', frame=frame)
    bpy.ops.object.mode_set(mode='OBJECT')

def adjust_scaling_factors(scaling_factors, target_volume,
   mesh, max_generations=300):
    current_volume = duplicate_mesh_and_calculate_volume(
       mesh)
    generation_count = 0

    while round(current_volume, 3) != round(target_volume,
       3) and generation_count < max_generations:
        for bone_name, factors in scaling_factors.items():
            scale_bone_and_mesh(armature, bone_name,
               factors['iteration'], frame=generation_count
               )
            factors['iteration'] = tuple(a - b for a, b in
               zip(factors['iteration'], factors['tolerance
               ']))

        bpy.context.view_layer.update()
        delete_mesh = generation_count < max_generations -
           1
        current_volume =
           duplicate_mesh_and_calculate_volume(mesh,
           delete_mesh)
        generation_count += 1
        print(f"Generation {generation_count}: Current
           volume = {current_volume}")

    return scaling_factors, current_volume,
       generation_count
```

```
# Calculate the percentage reduction for each part
def calculate_percentage_reduction(original, current):
    return (original - current) / original * 100

# Calculate the percentage left for each part
def calculate_percentage_left(reduction_percentage):
    return 100 - reduction_percentage

armature = bpy.data.objects['Armature']
mesh = bpy.data.objects['mesh']

original_volume = calculate_volume(mesh.data)
target_volume = original_volume * 0.75  # Change this to
   your desired proportion

scaling_factors = {
    'Head': {'iteration': (1, 1, 1), 'tolerance': (0.00039,
        0, 0.00039)},
    'Neck': {'iteration': (1, 1, 1), 'tolerance': (0.00143,
        0, 0.00143)},
    'Chest': {'iteration': (1, 1, 1), 'tolerance':
      (0.00178, 0, 0.00178)},
    'Abdomen': {'iteration': (1, 1, 1), 'tolerance':
      (0.00205, 0, 0.00205)},
    'Buttock': {'iteration': (1, 1, 1), 'tolerance':
      (0.00228, 0, 0.00228)},
    'Left_large_arm': {'iteration': (1, 1, 1), 'tolerance':
        (0.00156, 0, 0.00156)},
    'Right_large_arm': {'iteration': (1, 1, 1), 'tolerance
      ': (0.00156, 0, 0.00156)},
    'Right_small_arm': {'iteration': (1, 1, 1), 'tolerance
      ': (0.00078, 0, 0.00078)},
    'Left_small_arm': {'iteration': (1, 1, 1), 'tolerance':
        (0.00078, 0, 0.00078)},
    'Left_hand': {'iteration': (1, 1, 1), 'tolerance':
      (0.00039, 0, 0.00039)},
    'Right_hand': {'iteration': (1, 1, 1), 'tolerance':
      (0.00039, 0, 0.00039)},
```

```
    'Left_thigh': {'iteration': (1, 1, 1), 'tolerance':
      (0.00156, 0, 0.00156)},
    'Left_calf': {'iteration': (1, 1, 1), 'tolerance':
      (0.00078, 0, 0.00078)},
    'Left_foot': {'iteration': (1, 1, 1), 'tolerance':
      (0.00039, 0, 0.00039)},
    'Right_thigh': {'iteration': (1, 1, 1), 'tolerance':
      (0.00156, 0, 0.00156)},
    'Right_calf': {'iteration': (1, 1, 1), 'tolerance':
      (0.00078, 0, 0.00078)},
    'Right_foot': {'iteration': (1, 1, 1), 'tolerance':
      (0.00039, 0, 0.00039)},
}

adjusted_scaling_factors, final_volume, generation_count =
   adjust_scaling_factors(scaling_factors, target_volume,
   mesh)

print("Original volume:", original_volume)
print("Final volume:", final_volume)
print("Generation count:", generation_count)

print("\nResults:\n")
for bone_name, factors in adjusted_scaling_factors.items():
    original_scale = (1, 1, 1)
    reduction_percentages = [calculate_percentage_reduction
      (o, c) for o, c in zip(original_scale, factors['
      iteration'])]
    percentages_left = [calculate_percentage_left(p) for p
      in reduction_percentages]

    print(f"{bone_name}:")
    print(f"    final scale = {factors['iteration']}")
    print(f"    reduction percentages = {
      reduction_percentages}")
    print(f"    percentages left = {percentages_left}")
    print("\n")
```

Appendix B

Skin Fold Simulation Code

```
import bpy
import bmesh

mesh = bpy.data.objects['mesh']

# Mass levels mapping for different vertex groups
mass_levels = {
    'Arm': [300, 600, 1000, 1500],
    'Thighs': [300, 800, 1500],
    'Abdomen': [1000, 2000, 4000, 8000],
    'Mammary Gland': [500, 1000, 2000]
}

# Select the 'Fold' vertex group and scale it
vertex_group_fold = mesh.vertex_groups['Fold']
for v in mesh.data.vertices:
    for g in v.groups:
        if g.group == vertex_group_fold.index:
            scale_factor = 1 + 0.15 * g.weight
            v.co.x *= scale_factor
            v.co.z *= scale_factor

print("Scaling of 'Fold' vertex group completed.")

# Combine 'Fold' and 'Arm' into a new vertex group 'Skin'
vertex_group_other = mesh.vertex_groups['Arm']
vertex_group_skin = mesh.vertex_groups.new(name='Skin')
```

```
for v in mesh.data.vertices:
    for g in v.groups:
        if g.group == vertex_group_fold.index or g.group ==
            vertex_group_other.index:
            vertex_group_skin.add([v.index], weight=1, type
               ='ADD')

print("Creation of new vertex group 'Skin' completed.")

# Create new vertex group "Pin" and set weights to vertices
    not in 'Skin'
vertex_group_pin = mesh.vertex_groups.new(name='Pin')

for v in mesh.data.vertices:
    if vertex_group_skin.index not in [g.group for g in v.
       groups]:
        vertex_group_pin.add([v.index], weight=1, type='ADD
           ')

print("Creation of new vertex group 'Pin' completed.")

# Apply cloth physics system
cloth = mesh.modifiers.new(name='Cloth', type='CLOTH')
cloth.settings.vertex_group_mass = 'Pin'

# Set mass based on the selected vertex group
selected_vertex_group = vertex_group_other.name  # or any
   name you choose
cloth.settings.mass = mass_levels[selected_vertex_group][0]
    # Assuming you choose level 1 by default
cloth.settings.tension_stiffness = 15
cloth.settings.compression_stiffness = 2
cloth.settings.bending_stiffness = 0.5
cloth.settings.shear_stiffness = 40

print("Application of cloth physics system completed.")

# Simulate cloth physics effect
```

```
bpy.context.scene.frame_set(100)

print("Simulation and display completed.")
```